
Research Article: New Research | Novel Tools and Methods

Optogenetic control of spine-head JNK reveals a role in dendritic spine regression

<https://doi.org/10.1523/ENEURO.0303-19.2019>

Cite as: eNeuro 2020; 10.1523/ENEURO.0303-19.2019

Received: 30 July 2019

Revised: 18 December 2019

Accepted: 19 December 2019

This Early Release article has been peer-reviewed and accepted, but has not been through the composition and copyediting processes. The final version may differ slightly in style or formatting and will contain links to any extended data.

Alerts: Sign up at www.eneuro.org/alerts to receive customized email alerts when the fully formatted version of this article is published.

Copyright © 2020 Hollos et al.

This is an open-access article distributed under the terms of the Creative Commons Attribution 4.0 International license, which permits unrestricted use, distribution and reproduction in any medium provided that the original work is properly attributed.

1 **1. Manuscript Title:** Optogenetic control of spine-head JNK reveals a role in dendritic spine
2 regression

3 **2. Abbreviated title:** JNK drives dendritic spine shrinkage

4
5 **3. List all Author Names and Affiliations in order as they would appear in the published**
6 **article**

7
8 Patrik Hollos¹, Jismi M. John, Jukka V. Lehtonen², Eleanor T. Coffey^{1#}

9 ¹*Turku Bioscience, Åbo Akademi University and University of Turku, Biocity, Tykistökatu 6, Turku*
10 *FI-20500, Finland.*

11 ²*Biochemistry, Faculty of Science and Engineering, Åbo Akademi University, Artillerigatan 6, FI-*
12 *20500, Åbo, Finland*

13
14 **4. Author Contributions:** P.H. and J.J. carried out experimental work. J.V.L. and E.T.C. provided
15 expert guidance. All authors gave intellectual input.

16 **5. Correspondence should be addressed to (include email address):** *Eleanor Coffey, Turku*
17 *Bioscience, University of Turku and Åbo Akademi University, Biocity, Tykistökatu 6, Turku FI-*
18 *20500, Finland. (Tel) 358-40-1822424, (email) ecoffey@bioscience.fi*

19
20 **6. Number of Figures:** 6+5 extended figures (1-1; 2-1; 2-2; 3-1; 4-1)

21
22 **7. Number of Tables:** 0

23
24 **8. Number of Multimedia:** 2 movie files (.mp4)

25
26 **9. Number of words for Abstract:** 168

27
28 **10. Number of words for Significance**
29 **Statement:** 119

30
31 **11. Number of words for Introduction:** 625

32
33 **12. Number of words for Discussion:** 1252

34
35 **13. Acknowledgements:** We thank the Cell Imaging Core at Turku Bioscience for providing
36 technical support.

37
38 **14. Conflict of Interest:** Authors report no conflict of interest

39
40 **15. Funding sources:** This work was funded by Academy of Finland grant #135090 and EU FP7
41 ITN #608346 rBIRTH to E.C. and the Molecular Biology Graduate School at Åbo Akademi
42 University who funded P.H.

43 **16. Ethics statement:** Animal procedures were performed in accordance with the Turku Central
44 Animal Laboratory regulations and national guidelines.

45
46

47 **Optogenetic control of spine-head JNK reveals a role in dendritic spine regression**

48

49 Running title: **JNK drives dendritic spine shrinkage**

50

51 ABSTRACT

52 In this study, we use an optogenetic inhibitor of JNK in dendritic spine sub-compartments of rat
53 hippocampal neurons. JNK inhibition exerts rapid (within seconds) reorganisation of actin in the
54 spine-head. Using real-time FRET to measure JNK activity, we find that either excitotoxic insult
55 (NMDA) or endocrine stress (corticosterone), activate spine-head JNK causing internalization of
56 AMPARs and spine retraction. Both events are prevented upon optogenetic inhibition of JNK, and
57 rescued by JNK inhibition even 2 h after insult. Moreover, we identify that the fast-acting anti-
58 depressant ketamine reduces JNK activity in hippocampal neurons suggesting that JNK inhibition
59 may be a downstream mediator of its anti-depressant effect. In conclusion, we show that JNK
60 activation plays a role in triggering spine elimination by NMDA or corticosterone stress, whereas
61 inhibition of JNK facilitates regrowth of spines even in the continued presence of glucocorticoid.
62 This identifies that JNK acts locally in the spine-head to promote AMPAR internalization and spine
63 shrinkage following stress, and reveals a protective function for JNK inhibition in preventing spine
64 regression.

65 *168 words*

66

67 SIGNIFICANCE STATEMENT

68 Identifying mechanisms that underlie dendritic spine elimination is important if we are to
69 understand maladaptive changes that contribute to psychiatric disease. Compartment-specific, fast-
70 acting tools can expedite this endeavor. Here we use a light-activated inhibitor of JNK to control
71 kinase activity specifically in dendritic spines. Light-activation of the JNK inhibitor reduces AMPA
72 receptor removal and spine regression in response to corticosterone and NMDA stress. Furthermore,
73 we find that the anti-depressant drug ketamine lowers JNK activity in hippocampal neurons and
74 prevents spine regression, though direct JNK inhibition is more effective. This study identifies a

- 75 role for JNK in spine regression and may be relevant for endocrine control of synaptic strength and
76 for conditions where chronic glucocorticoid stress leads to spine elimination.

77

78 INTRODUCTION

79 Dendritic spines account for more than 90 % of glutamatergic synapses in the brain and are
80 essential sites for processing electrochemical input (Nimchinsky et al., 2002). New spine growth
81 and synapse formation occur throughout life and stabilization of synapses correlates with memory
82 formation and consolidation (Matsuzaki et al., 2001; Noguchi et al., 2011; Attardo et al., 2015;
83 Berry and Nedivi, 2017). Turnover of spines also effects learning and memory performance and
84 transient spines permit Hebbian-like plasticity (Holtmaat and Caroni, 2016). On the other hand,
85 excessive spine elimination is a hallmark of schizophrenia and major depressive disorder (Musazzi
86 et al., 2011; Duman and Duman, 2015; Varidaki, 2016; Wohleb et al., 2018), and post mortem
87 studies report that there are spine deficits in prefrontal cortex and hippocampus of these individuals
88 (Michelsen et al., 2007; Duman, 2009; Hajszan et al., 2009; Duman et al., 2011; Duman and
89 Aghajanian, 2012; Radley et al., 2013). In addition to this, classical anti-depressant drugs such as
90 fluoxetine and desipramine have been shown to reverse spine loss (Chen et al., 2009; Hajszan et al.,
91 2009; Rubio et al., 2013; McAvoy et al., 2015) suggesting that spine loss may contribute to the
92 underlying pathology. Even the fast-acting anti-depressant ketamine has been shown to prevent net
93 spine loss in a rodent chronic stress model, leading to recovery of dysfunctional circuit activity
94 (Moda-Sava et al., 2019; Treccani et al., 2019). Thus spine regression while a fundamental feature
95 of normal synaptic plasticity, is also associated with psychiatric disorders. Molecular drivers of
96 spine shrinkage are largely unknown.

97

98 c-Jun NH₂-terminal kinases (JNKs) exert pleiotropic functions during development of the nervous
99 system, regulating cell death and proliferation as well as migration and dendrite arborization
100 (Weston and Davis, 2007; Westerlund et al., 2011; Bjorkblom et al., 2012; Coffey, 2014;
101 Komulainen et al., 2014). However JNKs are first and foremost recognized as stress-activated

102 protein kinases that are strongly activated by a variety of cellular stresses including cytokines and
103 glucocorticoids (Qi et al., 2005; Kyriakis and Avruch, 2012), and stress-activated JNK is associated
104 with synaptic deficits in mouse models of Alzheimer's disease (Sclip et al., 2014). Moreover,
105 activation of JNK2 and 3 in hippocampus was shown to be necessary for stress-induced learning
106 deficit in mice (Sherrin et al., 2010). It has also been shown that interleukin, β -amyloid and
107 restraint-stress-induced activation of JNK impairs hippocampal LTP (Curran et al., 2003; Costello
108 and Herron, 2004; Sherrin et al., 2011). Evidence from animal studies and human genetics studies
109 suggest that dysregulation of the JNK pathway may be linked to psychiatric disorders (Winchester
110 et al., 2012; Kunde et al., 2013; Mohammad et al., 2016; McGuire et al., 2017; Kowalchuk et al.,
111 2019; Openshaw et al., 2019b). For example, inhibition or genetic deletion of *Jnk1* reduces anxiety
112 and depressive-like behaviors in mice (Mohammad et al., 2016), and MAP2K7 heterozygote mice
113 display brain imaging endophenotypes and behaviors related to schizophrenia (Openshaw et al.,
114 2019a). Although JNK has been shown to regulate synaptic plasticity in learning and the JNK
115 pathway is genetically associated with disorders of synaptic function; mechanistic study of JNK
116 function in dendritic spines has been limited due to lack of tools that allow spatiotemporal control
117 of the kinase solely in the spine-head.

118

119 Here we exploit an optogenetic inhibitor of JNK to control kinase activity in spines. This reveals
120 that stress activated JNK triggers AMPA receptor internalization and rapid spine retraction
121 following activation by NMDA or corticosterone. The antidepressant drug ketamine, suppresses
122 activation of JNK and helps prevent spine loss, however direct JNK inhibition elicits a faster and
123 more potent block of receptor internalization and spine retraction and reduces spine elimination
124 even when administered 2 h after glucocorticoid stress. These results indicate that JNK drives
125 dendritic spine regression in response to stress.

126

127 MATERIALS AND METHODS

128 *Plasmid construction* – Rat β -actin was obtained by PCR and was ligated to the EcoRI site of the
129 pVenus vector followed by exchanging the Venus tag for mCherry using NheI/BsrGI sites. NES-c-
130 Jun(1-146) was prepared by PCR based methods from pcDNA3-mJIP1a (Flag-JBD) (gift from
131 Martin Dickens, Leicester) and cloned into eGFP-C1 (Clontech, CA, US). Subsequently, GFP was
132 replaced for mCherry using NheI/BsrGI sites to yield mCherry-NES-c-Jun(1-146). The photo-
133 activatable pLuc-LOV2WTJ α WT-JBD (*LOV2-JBD*), the *lit-state* mutant pLuc-LOV2WTJ α IE-JBD
134 and the *dark-state* mutant pLuc-LOV2C450AJ α WT-JBD, were prepared by ligating JNK
135 interacting protein-1 (JIP1 144-154) “RPKRPTTLNLF” downstream of LOV2 to generate a
136 specific inhibitor of JNK, as previously described (Melero-Fernandez de Mera et al., 2017). LOV2
137 was generated by gene synthesis from *Avena sativa* LOV2 with codon optimization. GFP-
138 LOV2WTJ α WT (LOV2-JBD) was prepared by PCR insertion of wild-type LOV2 into the pEGFP-
139 C1 vector with overhanging SalI/SacII sites. To generate a red-shifted FRET sensor that would not
140 overlap with the LOV2 absorption peak, the JNKAR1EV probe (provided by Michiyuki Matsuda,
141 Kyoto University) was modified by inserting mRuby2 and Clover tags (gifts from Michael Lin,
142 Addgene plasmids #40260 and #40259 respectively), in place of ECFP and YPET using
143 EcoRI/XhoI and NotI/SalI sites respectively. pCI-SEP GluR2 (SEP-GluR2) was a gift from Robert
144 Malinow (Addgene plasmid # 24001) and eYFP-C1 was from Clontech, CA US.

145

146 *Structure prediction* - To generate an estimated view of possible 3 dimensional conformations of
147 the LOV2-JBD tools in dark and lit states, we used MODELLER (Sali and Blundell, 1993). This
148 software uses known Protein Data Bank-derived structures as templates for prediction of least
149 constrained conformations, and is reported to generate chemically correct models (Wallner and
150 Elofsson, 2005). PDB ID 2VOU and 2V1A cryo-trapped wild-type and *dark-state* structures of

151 LOV2 (Halavaty and Moffat, 2007) were used as templates to predict the dark-state after alignment
152 with our *dark-state* mutant. PDB ID 2V0W and 2V1B were used as templates for the *lit-state*
153 mutant (Heo et al., 2004). Energy minimization utilized “Yet another Scientific Artificial Reality
154 Application” (YASARA v16) (Krieger et al., 2009). α atoms were aligned with templates to
155 obtain root mean squared deviation (RMSD) values for the models. The top hit energy minimized
156 model from MODELLER v9.11 was used.

157

158 *Immunocytochemistry and wide field imaging* - Phosphorylated c-Jun (p-Jun) was detected using
159 (1:200) anti-phospho-c-Jun Ser 63 II (# 9261) from Cell Signaling Technology (Danvers, MA,
160 USA), which has been shown to be specific (Brecht et al., 2005) and detected with anti-rabbit-
161 Alexa-488, -568 or -405 (1:500) as indicated, from Invitrogen Corporation (Carlsbad, California).
162 Hoechst-33342 and Mowiol mounting media were from Molecular Probes (Eugene, OR, USA). For
163 immunostaining, neurons grown on 13 mm coverslips were washed once with 1 ml ice cold PBS
164 and fixed using 4 % PFA for 30 min. After 3 x 1 ml washes with PBS, cells were permeabilized
165 using 1 % Triton-X in PBS for 3 min and washed again (3 x 1 ml) with PBS. Non-specific binding
166 was blocked using 10 % fetal bovine serum for 1 h. Primary and secondary antibodies were added
167 consecutively, each for 1 h incubations. Coverslips were mounted in 8 μ l Mowiol containing
168 DABCO anti-fade and analyzed using a Zeiss LSM-780 with appropriate laser illumination.
169 Imaging of p-c-Jun and mCherry-NES-Jun was carried out with a Leica DMRE upright microscope
170 and 40x air objective. Identical acquisition parameters were used for all cells so that the images
171 were quantitatively comparable. Line intensities (15 μ m) were measured from the dendritic shaft
172 using ImageJ (NIH, Bethesda, US). Cytoplasmic JNK activity was calculated from non-saturated
173 line intensity ratios: [intensity p-Jun] / [intensity mCherry-NES-Jun]. Ratiometric images were
174 generated using the Ratio Plus plugin for ImageJ.

175

176 *Hippocampal neuron isolation and maintenance* - Newborn Sprague-Dawley rats of either sex were
177 decapitated and the hippocampus rapidly removed into *dissection media* (1 M Na₂SO₄, 0.5 M
178 K₂SO₄, 1 M MgCl₂, 100 mM CaCl₂, 1 M Hepes (pH 7,4), 2,5 M Glucose, 0,5 % Phenol Red).
179 Meninges were removed and tissue pieces collected into *dissection media* containing 10 % KyMg,
180 followed by washing. Tissues were incubated with 10 U/ml papain (Worthington, 3119) for 15 min
181 at 37°C, repeated two times. Papain was inactivated by incubation with 10 mg/ml trypsin inhibitor
182 (Sigma, T9128) for 2 x 5 min at 37°C. Tissue was then dissociated by trituration to yield a
183 homogenous solution of cells. Cultures were maintained in Neurobasal-A (Thermo Fisher
184 Scientific), supplemented with 2 mM glutamine, 50 U/ml penicillin, 50 µM streptomycin and B27
185 Neuronal supplement (Gibco, Thermo Fisher Scientific). Cells were transfected with a DNA mix
186 comprising 30 % of transgene vector and 70 % of pCMV vector lacking transgene, to give a total of
187 0.5 µg DNA per 24-well plate well, using 7-10 days *in vitro* (DIV) cells using Lipofectamine 2000
188 (Thermo Fisher) following the manufacturer's instructions. Experiments were carried out in
189 hippocampal pyramidal cells at 16-18 DIV.

190
191 *Photo-activation of LOV2 variants* - Cells for live cell imaging were plated on glass bottom dishes
192 (Greiner Bio-One GmbH, DE) or in black walled glass bottom dishes (PELCO, Ted Pella, US),
193 when light sensitive constructs were used. Cells transfected with photosensitive constructs were
194 protected from ambient light in a foil-covered dark box for 5 min prior to imaging. Handling was
195 performed in a darkened room where the computer monitor was set on minimum light level for set-
196 up and switched off during experiments. In experiments where photo-activation was used and
197 subsequently monitored, we used a Zeiss LSM-780 or Zeiss LSM-880 with Airyscan microscope,
198 as indicated. This was equipped with an incubator chamber: 37 °C, 5% CO₂ and 10x objective was
199 used with a 458 nm argon laser, scan speed of 1.68 µs/pixel in "live scan" mode for 30 s, followed
200 by immediate fixation with 4 % PFA. 3% laser power, (0.4 mW irradiance) was used for LOV2

201 illumination, unless otherwise indicated. Regions of interest in dendritic spines were illuminated
202 with the 458 nm laser for 1 s with 1.68 μ s/pixel dwell speed using 63x 1.2 W objective. For Fig. 1F,
203 where field illumination was used, hippocampal neurons in a 24-well plate were illuminated by
204 placing 40 cm below a fluorescent lamp (Phillips, PL-2 11W/865/2P ICT/25) for 30 s followed by
205 immediate fixation of cells with 4% PFA.

206

207 *FRET imaging and analysis* - FRET analysis was performed using the Zeiss FRET module. *Control*
208 (acceptor or donor alone) and *FRET* images were acquired by using the Lambda stack scan mode on
209 the Zeiss-LSM 780 to achieve appropriate spectral separation. For mRuby2-JNKAR1EV-Clover
210 FRET imaging, the donor (Clover) was excited with 488 and 0.4 mW irradiance measured at the
211 objective (63x). and mRuby2 was imaged using 543 nm excitation and 0.24 mW irradiance
212 measured at the objective which was 63x. When LOV2-JBD was present, 458 nm laser excitation
213 was used with 0.4 mW irradiance measured at the 63x objective. To calculate FRET efficiency,
214 several regions of interest were drawn on dendrites and Youvan's method was used to calculate the
215 FRET response as follows: $F_c = (fret_{gv} - bg_{fret}) - cf_{don} * (don_{gv} - bg_{don}) - cf_{acc} * (acc_{gv} - bg_{acc})$, where: F_c =
216 FRET concentration, gv = gray value intensity, bg = background intensity, don = donor image, acc
217 = acceptor image, cf = correction factor. To compare FRET efficiency between different cellular
218 compartments, normalized FRET (N-FRET) values were calculated as following N-FRET: F_f -
219 $([don_{corr}] - [acc_{corr}]) / \sqrt{[(G(F_d)(F_a))]}$, where F_f the FRET image in FRET channel, don_{corr} = donor
220 image with donor excitation, acc_{corr} = acceptor image with acceptor excitation, F_d = emission
221 crosstalk of the Donor in the FRET channel, F_a = emission crosstalk of the Acceptor in the FRET
222 channel, G = Donor emission factor in the Donor channel due to FRET, relative to the acceptor
223 emission due to FRET in the FRET channel.

224

225 *Measurement of actin dynamics in dendritic spines* - Hippocampal neurons expressing mCherry-
226 actin (or GFP-actin as indicated) together with LOV2 variants (as indicated), were imaged using a
227 Zeiss-LSM 780 (or LSM-880 in Airyscan mode where indicated) microscope and a 63x objective
228 (C-Apochromat, 1.2 numerical aperture) for live cell imaging or with a Zeiss LSM-880 Airyscan
229 microscope for live-cell 3D imaging of spines. A 543 nm laser at 3 % power was used to image
230 mCherry-actin, and a 488 nm laser at 6 % power for GFP-actin (Fig. 2 only), in dendritic spines
231 from secondary dendrites, located 20-30 μm from the soma were measured. The stack registration
232 plugin from ImageJ was used to correct x, y drift from time-lapse series and images were then
233 median filtered with 1-pixel radius to enhance the signal-to-noise ratio. Scan speed was 1.68
234 $\mu\text{s}/\text{pixel}$ and the time between frames was 6 s. For fast 3D Zeiss LSM-880 Airyscan imaging, scan
235 speed was approx. 150 ms for every 0.22 μm z-slice. Photo-activation of LOV2-constructs was
236 achieved using the 458 nm laser line at 3% laser power (0.4 mW irradiance).

237

238 The motility of GFP, mCherry-actin or YFP within spines was quantified using arithmetic
239 difference projection analysis as described by (Fischer et al., 1998; Bjorkblom et al., 2012).
240 Displacement images were generated between consecutive frames of 6 s interval and the sum of all
241 displacement is projected. These provided a 2D quantitative view of movement across the time
242 frame where pixel intensity corresponds to actin displacement. Arithmetic projections were inverted
243 for visualization. The “motility index” describes the average intensity in regions of interest from
244 arithmetic projections. The “motility ratio” was the ratio of motility indices obtained before and
245 after light activation. To view the temporal detail of dynamic changes, RGB temporal color coded
246 difference projections were generated using frame-by-frame difference stacks. For this we used the
247 ImageJ Hyperstack color-code plugin with customized LUT. A white, or Gaussian mix of colors
248 indicates continuous motility. Each time frame is represented by a unique hue. For these fast

249 motility measurements, LSM-880 Airyscan images were acquired in fast-scan mode, taking a 6 x 6
250 x 4 (XYZ) μm voxel scan approximately every second.

251

252 *Measurement of synaptic GluR2 receptors and spine-head volume* - To measure surface GluR2

253 levels at synapses, hippocampal neurons expressing SEP-GluR2 (which undergoes fluorescence

254 quenching upon internalization into endocytic vesicles) and mCherry-Actin underwent time-lapse

255 imaging for 40 min using the Zeiss LSM-880 in Airyscan mode using the 488 nm laser at 0.8 %

256 (0.19 mW) power so as to minimize inadvertent photo-activation of LOV2. Fluorescence intensity

257 for each fluorescent protein was measured from circular regions of interest in spines. To determine

258 relative GluR2 surface expression, the ratio of SEP-GluR2 to mCherry-Actin or YFP was

259 calculated. To analyze spine head volume, r.o.i. voxels were drawn encompassing the entire volume

260 occupied by visible mCherry-Actin or YFP in the spine head throughout the time lapse as

261 previously (Basu et al., 2018; Hruska et al., 2018), ensuring that the entire 4D footprint was

262 included in the analysis. The z-depth was 4 μm and x, y dimensions varied according to individual

263 spine size. Spines were imaged in 3D with a z-section of 0.2 μm scan speed of 3 frames per s.

264 Relative changes in dendritic spine volume were estimated from maximum intensity projections

265 from these images. To calculate a baseline spine volume, maximum projections from 3 min of

266 image acquisition prior to treatment were averaged. Subsequent recordings were normalized to this

267 value. For fixed cell analysis, relative changes in dendritic spine volumes and SEP-GluR2 to

268 mCherry-Actin ratios were normalized to control conditions (before treatment). Boundaries of spine

269 heads were drawn from maximum intensity images where the border was defined by change in

270 signal:noise >10 compared to mean background.

271

272 *Hippocampal neuron pharmacological treatments* - Anisomycin (Sigma) was added at 10 μM

273 concentration in growth media to hippocampal neurons during live cell imaging after 5 min of

274 baseline recording. To produce chemical long-term depression, hippocampal neurons at 16-18 days
275 *in vitro* were treated with 20 μ M NMDA (Tocris Biosciences, UK) for 3 min in Neurobasal-A, after
276 which conditioned growth medium was added back, as previously described (Lee et al., 1998).
277 Corticosterone (100 nM; Sigma-Aldrich Finland Oy) was added to hippocampal neurons following
278 5 min of baseline recording or 2 h before or after ketamine treatment as indicated. Ketamine (10
279 μ M; Tocris Biosciences, UK) was added to hippocampal neurons 2 h prior to recording. Latrunculin
280 B (1 μ M; Sigma-Aldrich Finland Oy) or Phalloidin (500 nm; Sigma-Aldrich Finland Oy) were
281 added to hippocampal neurons following 5 min of baseline recording.

282

283 *Statistical analysis* – Student’s two-tailed t-tests were used to calculate *p*-values where two groups
284 were compared. Repeated measures one-way ANOVA was used to compare multiple groups and *p*-
285 values were corrected by Bonferroni correction. Error bars represent standard errors of the mean
286 (S.E.M.). In each case, measurements were taken from multiple cells and spines from separate
287 experiments, and statistical analysis is detailed in the corresponding legend.

288

289

290
291 RESULTS

292 We generated an optically controllable inhibitor of JNK to enable localized inhibition of JNK
293 function exclusively in dendritic spines without altering JNK activity in other compartments. To do
294 this, we replaced the kinase domain from *Avena sativa* phototropin with an 11-mer peptide inhibitor
295 of JNK (JNK binding domain; JBD), a highly specific peptide inhibitor of JNK which does not
296 inhibit other MAPKs (Bonny et al., 2001; Borsello et al., 2003) (Fig. 1A). We hypothesized that in
297 the absence of light, steric hindrance conferred by a constrained $J\alpha$ helix would prevent JBD from
298 binding and inhibiting JNK, thereby allowing unhindered function of the kinase within the cell.
299 Conversely, upon illumination, relaxation of the $J\alpha$ helix should release this constraint and facilitate
300 kinase inhibition.

301

302 **An optically controlled JNK inhibitor assumes an inward-pointing, constrained dark-state**
303 **and outward-pointing extended lit-state conformation**

304 To validate LOV2-JBD as a light-regulated JNK inhibitor, we used a *dark-state* mutant of LOV2
305 encoding a C450A mutation in the photo-sensing domain to impose a constrained conformation
306 (Salomon et al., 2000), and a *lit-state* mutant with I539E mutation in the $J\alpha$ helix, that imposes a
307 relaxed conformation (Harper et al., 2004) (Fig. 1B). Using homology modelling, we found that
308 both *lit-* and *dark-state* mutant $C\alpha$ atoms aligned well to the crystallographic reference structure for
309 LOV2 with RMSDs of 0.52 Å and 0.57 Å respectively (Fig. 1C). Also, the top 5 $J\alpha$ helix models
310 retained 6 α -helical turns consistent with crystallographic and NMR *Avena sativa* LOV2 (Halavaty
311 and Moffat, 2007; Peter et al., 2010). However, the tandem-encoded 11-mer JBD switched from an
312 inward pointing α -helix in the *dark-state* mutant to an extended conformation that projected away
313 from LOV2 in the *lit-state* mutant (Fig. 1C). Notably, the relaxed conformation of the *lit-state*
314 mutant JBD was similar to the structure of JIP1(11) bound to JNK1 (Heo et al., 2004), consistent
315 with this being an inhibitory conformation (Fig. 1D). Alignment of $C\alpha$ atoms gave an overall

316 RMSD of 1.68Å, indicating close alignment between the structures (Fig. 1C, 1D). These data
317 predicted that the LOV2-JBD light sensing J α helix would undergo a conformational change upon
318 blue light exposure analogous to that of phototropin-LOV2 (Peter et al., 2010; Fig 1), leading to a
319 relaxed JBD inhibitor conformation, suitable for trans-inhibition of enzymatic activity (Heo et al.,
320 2004).

321

322 **Proof of concept that LOV2-JBD inhibits JNK in response to light**

323 To test experimentally whether LOV2-JBD could be induced by light to inhibit JNK in
324 hippocampal cells, we first measured the phosphorylation of mCherry-NES-Jun as a surrogate
325 reporter of JNK activity in the cytoplasm of transfected cells. Hippocampal neurons displayed
326 elevated phosphorylation of mCherry-NES-Jun, consistent with the high basal activity of JNK in
327 the cytosol that is characteristic of neurons (Coffey et al., 2000; Coffey, 2014). In cells expressing
328 LOV2-JBD, photo-activation using 458 nm laser substantially reduced JNK activity (Fig. 1E).
329 Importantly expression of GFP-LOV2 alone did not alter JNK activity (Fig. 1F), indicating that the
330 JBD sequence was required and that LOV2 alone did not affect JNK activity.

331

332 **JNK is catalytically active in dendritic spines and can be optically controlled**

333 To visualize real-time JNK activity in neurons, we modified an intramolecular Förster Resonance
334 Energy Transfer (FRET) reporter (JNKAR1EV) (Komatsu et al., 2011) by substituting
335 mRuby2/Clover for the ECFP/YPET FRET pair to generate a reporter that had increased sensitivity
336 (Extended Data Fig. 2-1 A-B), and minimal spectral overlap with LOV2-JBD. Baseline
337 measurements in hippocampal neurons indicated that JNK activity was elevated not only in
338 dendrites, as previously shown (Björkblom et al., 2005), but also in dendritic spines (Fig. 2A). After
339 treatment with anisomycin, an activator of JNK (Cano et al., 1994), FRET activity increased further
340 in dendrites and spines (Fig. 2B-D), whereas upon expression of the Flag-JBD inhibitor, reporter

341 activity decreased by 90 % (Fig. 2E, F). These data indicate that mRuby2-JNKAR1EV-Clover
342 provides a sensitive and specific measure of JNK activity in living neurons. We next used mRuby2-
343 JNKAR1EV-Clover to test optogenetic inhibition of JNK. Photo-stimulation of LOV2-JBD using
344 458 nm illumination decreased FRET reporter activity by 50% (Fig. 2E, F), whereas in cells
345 expressing FRET reporter alone, 458 nm illumination had no effect (control), indicating that light-
346 induced inhibition of JNK FRET reporter activity required LOV2-JBD. In these experiments, we
347 did observe a moderate inhibition of JNK activity in cells expressing LOV2-JBD merely upon 488
348 nm excitation of mRuby2-JNKAR1EV-Clover. The extent of inhibition was 30%, as validated also
349 with an independent JNK activity reporter (Extended Data Fig. 2-2).

350

351 **JNK activity regulates dendritic spine motility**

352 The effect of JNK on dendritic spine motility was measured using arithmetic difference projection
353 images of GFP-actin generated from a time-series (Fig. 2G). Dendritic spines were highly motile in
354 16 day in vitro hippocampal neurons, in cells expressing Flag-JBD, spine-head movement was
355 blocked (Fig. 2G, H). Cells expressing the *lit-state* LOV2-JBD mutant also exhibited reduced
356 motility, whereas neurons expressing the *dark-state* mutant which fails to inhibit JNK (Extended
357 Data Fig. 1-1 A-B), did not show altered dynamics (Fig. 2G, H). We found that a relatively low
358 irradiance of 0.4 mW was sufficient to reduce spine motility (Fig. 2I), and we utilized this
359 “threshold” setting for photo-activation of LOV2-JBD from here on so as to avoid photo-toxic
360 effects.

361

362 **JNK acts locally within the spine-head to control spine motility**

363 We next exploited the spatiotemporal control of optogenetic inhibition to examine JNK regulation
364 of spine motility in more detail by specifically illuminating the inhibitor in the spine-head. In the
365 absence of 458 nm light, there was rapid displacement of mCherry-actin in the head and neck of the

366 spine and prominent re-shaping or morphing (Fig. 3A). Selective region of interest photo-
367 stimulation of LOV2-JBD solely in the spine-head was sufficient to reduce mCherry-actin motility,
368 however cells expressing the *dark-state* LOV2-JBD mutant remained unaltered (Fig. 3A-C).
369 Notably, there was no change in motility observed in the proximal dendrite or in non-illuminated
370 spines (Fig. 3A-C), indicating that JNK exerts rapid control of actin movement from within the
371 spine-head (Extended Data Fig. 3-1 A).

372

373 **JNK controls motility of spines with small “head diameter to neck length” ratios**

374 Mature dendritic spines consist of large, mushroom-shaped protrusions; yet both thin and
375 mushroom spines can appear and disappear throughout adulthood and are important for synaptic
376 plasticity (Holtmaat et al., 2008). To define which spine-type is primarily regulated by JNK, we
377 analyzed spines of different size categories. We defined spines according to the average head
378 diameter to neck length ratio assumed by a given spine during the imaging sequence, as previously
379 (Murase et al., 2016). Interestingly, JNK inhibition reduced motility only in spines that had an
380 average head to neck ratio of between 0.2 and 1.5, corresponding to “thin” and “long thin” spines
381 (Fig. 3D). In contrast, photo-stimulation of LOV2-JBD in mushroom spines (head diameter:neck
382 length ratio > 3), did not alter dynamics, even when laser power was increased to account for larger
383 spine-head volume (Extended Data Fig. 3-1 B). This data indicates that JNK specifically regulates
384 the motility of thin spines.

385

386 **JNK exerts rapid control over spine motility**

387 Protein phosphorylation is a highly dynamic process. We therefore measured how quickly a photo-
388 activated JNK inhibitor (LOV2-JBD) could affect actin motility (Fig. 3E, F). In neurons expressing
389 LOV2-JBD, exposure to a 1 s pulse of 458 nm light was sufficient to rapidly inhibit mCherry-actin
390 motility within 6 s of photo-stimulation. Motility returned to baseline by 2 min (Fig. 3E). We used

391 temporal color coding to obtain spatiotemporal information on actin regulation. Time projection
392 images revealed that optogenetic inhibition of JNK halted actin dynamics by 2 s (blue) in the
393 periphery of the spine and movement did not resume in this region during 90 s of monitoring (Fig.
394 3G, H). Interestingly, actin motility decreased in a polarized fashion, starting on one side of the
395 spine-head (blue) and progressing to the opposite side by 5 s (green), whereas the core domain of
396 actin in the spine centre remained motile (white) upon JNK inhibition (Fig. 3H, Extended Data Fig.
397 3-1 C-E, Movie 1-2). These data suggest that JNK controls actin dynamics in the peripheral domain
398 of the spine.

399

400 To help understand the contribution of actin dynamics to the spine motility changes measured, we
401 treated neurons with either latrunculin (which binds G-actin and prevents polymerization), or
402 phalloidin (which binds and stabilizes F-actin) (Saito, 2009). Latrunculin treatment of neurons
403 reduced spine motility (Fig. 3I-J) and yielded a characteristic “blue” time projection image
404 suggesting that inhibition of F-actin formation reduced spine dynamics (Fig. 3K). In contrast,
405 phalloidin-treated neurons maintained spine motility (Fig. 3I-J) and showed a distribution of
406 movements throughout the 90 s monitoring (Fig. 3K). The temporal coding pattern observed with
407 optogenetic inhibition of JNK is similar to that obtained with latrunculin suggesting dissolution of
408 F-actin.

409

410 **JNK is activated by corticosterone leading to internalization of AMPAR and rapid spine** 411 **retraction**

412 We were interested to know whether JNK regulated spine retraction in the context of synaptic
413 pathology because JNK1 was recently reported to control depressive and anxiety-like behaviors in
414 mice (Mohammad et al., 2016; Hollos et al., 2018). We therefore used corticosterone, the principal
415 glucocorticoid stress hormone in mice, which stimulates retraction of dendritic spines in specific

416 brain regions (Liston and Gan, 2011). JNK activity was measured in hippocampal neurons
417 expressing mRuby2-JNKAR1EV-Clover as earlier (Fig. 2). Corticosterone (100 nM) increased JNK
418 activity within 10 min in dendritic and spine compartments (Fig. 4A, B).

419

420 As AMPA receptor removal from the synapse is an early event during spine shrinkage (Hanley,
421 2014), we next investigated whether corticosterone would affect this process. GluR2 endocytosis
422 was visualized as previously described (Kessels et al., 2009) using a pH-luorin-tagged SEP-GluR2
423 which loses fluorescence when internalized to the low pH endocytic vesicles. Corticosterone rapidly
424 (within 5 min) reduced levels of SEP-GluR2 fluorescence at the plasma membrane in the spine
425 head. Interestingly, this was completely blocked when JNK was inhibited by photo-activation (Fig.
426 4C, D). Moreover, photo-activation of LOV2-JBD prevented SEP-GluR2 internalization even when
427 started 20 min after addition of corticosterone (Fig. 4C, D).

428

429 We also measured the effect of corticosterone on spine-head volume. This decreased within 10 min
430 of treatment with the glucocorticoid (Fig. 4C, E). Optogenetic inhibition of JNK rescued spine
431 retraction even when light was applied 20 min after corticosterone (Fig. 4C, E). These data suggest
432 that JNK controls GluR2 removal and regression of spines in response to corticosterone. To assess
433 if effects of actin over-expression would skew the estimate of motility measurements, we also
434 measured volumes and GluR2 endocytosis levels using soluble YFP. Corticosterone induced rapid
435 reduction of SEP-GluR2 fluorescence and spine-head volume, both of which were rescued upon
436 optogenetic inhibition of JNK (Extended Fig. 4-1).

437

438 **NMDA activates JNK and induces rapid spine shrinkage**

439 The glutamatergic system is strongly implicated in depression (Sanacora et al., 2012). We therefore
440 examined JNK regulation by NMDA using FRET as earlier (Fig. 2B, 4A). NMDA activated JNK

441 within minutes in dendritic and spine compartments (Fig. 5A, B). Three-minute bath application of
442 NMDA followed by 10 min rest, induced rapid spine shrinkage that was prevented by photo-
443 stimulation of LOV2-JBD (Fig. 5C). We next tested anisomycin, a ribotoxin that strongly activates
444 JNK (Fig. 2B). Anisomycin treatment induced more than 40% reduction of spine area (Fig. 5D-F).

445

446 **Ketamine inhibits JNK and prevents spine retraction and SEP-GluR2 receptor removal**

447 As NMDA is strongly activated by JNK (Fig. 5), we tested whether the NMDA receptor antagonist,
448 fast acting anti-depressant ketamine, altered JNK activity. Indeed, JNK activity was significantly
449 reduced after 2 hours of ketamine treatment (Fig. 6A, B). However, ketamine did not prevent SEP-
450 GluR2 removal from spines, nor did it prevent spine retraction in response to corticosterone at this
451 time point (Fig. 6C-E). Because the timeline of these ketamine treatments was only 40 minutes, less
452 than the 2 hours required to inhibit JNK (Fig. 6A, B), we tested if a 2-hour pre-treatment with
453 ketamine would prevent corticosterone-induced spine retraction. This prevented corticosterone-
454 induced spine shrinkage and inhibited GluR2 removal (Fig 6F, G). Finally, we examined whether
455 treatment with ketamine or DJNKI-1 two hours following corticosterone could rescue GluR2
456 internalization and spine retraction. Interestingly, inhibition of JNK 2 hours after corticosterone
457 recovered spine volume and GluR2 homeostasis (Fig. 6 H, I). Ketamine treatment did not rescue at
458 this time-point, likely because there was insufficient time to achieve robust JNK inhibition. These
459 data show that prophylactic treatment with ketamine or JNK inhibitor prevents spine retraction and
460 GluR2 removal in response to corticosterone. Inhibition of JNK supports spine regrowth and
461 rescues corticosterone effects on molecular events in spines even in the continued presence of
462 corticosterone.

463

464

465 DISCUSSION

466 Structural plasticity of dendritic spines facilitates elimination and regrowth of synapses and
467 provides a fundamental process for adaptive neurotransmission. Understanding the underlying
468 mechanism is relevant for memory and learning but also for pathologies such as depression, where
469 significant spine loss is a hallmark (Duman and Duman, 2015; Musazzi et al., 2015; Varidaki,
470 2016). Here, we identify using an optogenetic approach, that catalytically active JNK controls spine
471 stability from within the spine-head. Using arithmetic difference projections to quantify mCherry-
472 actin displacements over time, we observe a clear reduction of movement in spines commencing
473 within seconds of LOV2-JBD photo-stimulation to inhibit JNK solely in the spine-head. This rapid
474 response indicates a proximal mechanism whereby JNK acts directly in the spine to suppress
475 motility. Full recovery of spine movement after photo-stimulation is ended takes about 2 min,
476 consistent with the photo-cycle of LOV2-JBD which lasts approximately 80s, after which a
477 constrained state for LOV2-JBD is expected to re-establish (Zayner and Sosnick, 2014).

478

479 Counterintuitively perhaps, rapid extinction of actin motility upon JNK inhibition is temporally
480 similar to that observed with the actin polymerization inhibitor latrunculin, but distinct from that
481 seen in cells treated with the actin stabilizing drug phalloidin. Therefore, it may be that inhibition of
482 JNK immobilizes actin in spines due to increased G-actin to F-actin ratio, consistent with an earlier
483 study that showed that JNK inhibition in neurons increases soluble actin levels (Bjorkblom et al.,
484 2012). We show that JNK predominantly regulates spines with smaller head to neck length ratios,
485 suggesting a more pronounced control of thin spines. This spine class emerge as motile protrusions
486 during new synapse formation, enriched with dynamic actin (Engert and Bonhoeffer, 1999; Lendvai
487 et al., 2000; Matsuzaki et al., 2004; Cingolani and Goda, 2008), and is prominent throughout life
488 during synapse formation (Fischer et al., 2000; Holtmaat et al., 2008). Our data establishes that
489 physiologically active JNK controls actin dynamics locally in thin spines.

490

491 We show using temporal color-coding that optogenetic inhibition of JNK alters the actin pool at the
492 periphery of the spine rather than in the central region closer to the base of the spine and neck. The
493 peripheral pool of F-actin in this region has been shown to turnover rapidly with a half-life of
494 around 10 s compared to the stable pool of cross linked F-actin at the spine center which has a half-
495 life of 17 minutes (Honkura et al., 2008; Kasai et al., 2010; Bertling et al., 2016). Interestingly, the
496 dynamic F-actin pool in the peripheral domain that JNK controls is the same pool that regulates
497 AMPA receptor membrane trafficking (Cingolani et al., 2008; Honkura et al., 2008), a central event
498 during synaptic plasticity changes (Huganir and Nicoll, 2013). Consistent with this, we find that
499 corticosterone-activated JNK facilitates rapid (within 5 min) removal of SEP-GluR2 from the spine-
500 head membrane prior to spine retraction. This is blocked upon optogenetic inhibition of JNK in
501 spines. As the GluR2 subunit is associated predominantly with functional synapses (Passafaro et al.,
502 2001), these thin spines that are controlled by JNK most likely represent immature synapses. Thus,
503 our data uncovers that JNK activity reduces spine-head actin dynamics in the peripheral domain
504 which is permissive for receptor removal. This mechanism may be relevant for long-term
505 depression and impaired short-term memory regulation by JNK where AMPA receptor removal
506 plays a central role in downregulation of synaptic function (Bevilaqua et al., 2003; Li et al., 2007;
507 Myers et al., 2012).

508

509 Prolonged hyperactivity of the Hypothalamic-Pituitary-Adrenal (HPA) axis leading to elevated
510 glucocorticoids is associated with psychiatric disorders, in particular depression and anxiety (Malhi
511 and Mann, 2018). Both endocrine and glutamate stress have been shown to induce synapse
512 regression and dendritic atrophy that can lead to maladaptive circuit changes and depressive
513 behaviors (Musazzi et al., 2011; Bennett and Thomas, 2014; Duman and Duman, 2015). In mice,
514 chronic corticosterone is used to model depression, although even acute stress can induce long term

515 pathological changes at synapses (Musazzi et al., 2018). Corticosterone treatment of mice was
516 previously shown to activate JNK in the hippocampus (Solas et al., 2013). Here using real-time
517 FRET to measure spatiotemporal JNK activation by corticosterone, we find that spine-head JNK is
518 activated within 10 min of treatment, followed by a second phase of activation after 20 min. This
519 could be a consequence of increased glutamate efflux which occurs following corticosterone
520 (Musazzi et al., 2010; Sanacora et al., 2012; Treccani et al., 2014; Musazzi et al., 2017), as we show
521 that the NMDA receptor activates spine-head JNK within this timeframe. The downstream effect of
522 corticosterone-activated JNK is the rapid removal of SEP-GluR2 from synapses which occurs by 5
523 min, followed by spine retraction commencing 10 min after corticosterone. Moreover, spine
524 regrowth after corticosterone treatment can be recovered in spines where JNK is inhibited, up to 20
525 min after corticosterone addition. These data indicate that JNK activity regulates early events
526 leading to spine retraction upon corticosterone stress, whereas inhibition of JNK promotes spine
527 regrowth, even under conditions of maintained endocrine stress.

528

529 Strengthening and weakening of synaptic transmission is controlled by NMDA. High frequency
530 stimulation of the NMDAR coincident with pre-synaptic activity induces spine growth and synapse
531 strengthening, whereas NMDA in the context of chemical-long-term depression induces spine
532 shrinkage (Zhou et al., 2004). Here we use the chemical long-term depression (LTD) protocol (Lee
533 et al., 1998) which is believed to mimic low level long lasting NMDA receptor stimulation leading
534 to down regulation of post-synaptic AMPARs and synapse regression (Lee et al., 1998; Lüscher and
535 Malenka, 2012). This LTD protocol induces a reduction in relative spine-head volume within 3
536 minutes which is completely rescued upon LOV2-JBD photo-activation. These results suggest that
537 JNK activation locally within the spine may facilitate LTD. Consistent with this possibility, JNK1
538 has been previously implicated in LTD both in inhibitor DJNKI1 and *Jnk1*^{-/-} knockout studies (Ge

539 et al., 2007; Li et al., 2007), although at least nuclear substrate c-Jun has been excluded from this
540 mechanism as Jun-AA mice undergo normal LTD (Seo et al., 2012).

541

542 We find that ketamine or inhibition of JNK inhibition promote hippocampal neuron spine recovery
543 and SEP-GluR2 receptor trafficking in response to corticosterone. Moreover, we identify that

544 ketamine treatment leads to run-down of JNK activity in a relatively slow and phasic manner.

545 Nonetheless, JNK inhibition may be a critical downstream mediator of ketamine action in spines.

546 The kinetics of ketamine action on spines lags behind that of JNK inhibition, consistent with JNK
547 inhibition being a necessary downstream event. Clearly more work will be needed to establish

548 whether JNK inhibition contributes to ketamine action on spines in hippocampus and to determine

549 if this action serves any consequence in circuit remodeling. Although ketamine regulation of spines

550 in prefrontal cortex has been dissociated from its behavioral effect in mice (Moda-Sava et al.,

551 2019), the relevance of ketamine or JNK inhibition on spine dynamics in hippocampus has not been

552 studied in the context of depression. It is worth noting however that like ketamine, *Jnk1* deletion or

553 JNK inhibition using the same peptide inhibitor that is encoded in our optogenetic tool, lowers

554 anxiety- and depressive-like behaviors in mice (Mohammad et al., 2016; Hollos et al., 2018).

555

556 Optogenetic inhibition of JNK has allowed us to identify that JNK controls the dynamics of spine-

557 head actin from within the spine where it confers control of corticosterone- and chemical-long term

558 depression-induced spine plasticity. These findings describe a previously unknown role for JNK in

559 structural plasticity of synapses in the context of endocrine stress where JNK triggers rapid receptor

560 removal and spine regression.

561 FIGURE LEGENDS

562 **Figure 1. Design and validation of the LOV2-JBD inhibitor.** **A.** Schematic showing activation
563 of LOV2 photo-domain from *Avena sativa* by light. The proposed mode of action of LOV2-JBD is
564 shown in the lower panel where an 11-mer peptide inhibitor of JNK is released from the constrained
565 conformation upon photo-stimulation, facilitating binding to and inhibition of JNK. **B.** Constructs
566 used in this study. **C.** Superimposed, top five *lit-state* model predictions for LOV2-JBD. In the top-
567 ranked model, JIP1(11) (magenta) takes on a relaxed conformation projecting away from the core.
568 **D.** JIP1(11) from the *lit-state* model (magenta) superimposed on the crystal structure of JIP1(11)
569 from the JNK1-JIP1 co-crystal (green). **E.** mCherry-NES-Jun fluorescence provides a surrogate
570 reporter of JNK activity in hippocampal neurons expressing mCherry-NES-Jun (control) or
571 mCherry-NES-Jun with LOV2-JBD. Reporter activity is fluorescence intensity of phosphorylated c-
572 Jun (P-Jun)/mCherry fluorescence intensity. Photo-stimulation of LOV2-JBD reduces JNK activity
573 in hippocampal neurons, however **F.** Photo-stimulation of GFP-LOV2 does not. Data on dark-state
574 and lit-state mutants is in **Extended Data Figure 1-1**. Mean data +/- S.E.M. and Student's t test *p*-
575 values are shown. Cell numbers (from at least two experimental repeats) are indicated on the bars.
576

577 **Figure 2. Photo-activation of LOV2-JBD reduces actin dynamics in dendritic spines.** **A.**
578 Hippocampal neurons expressing mRuby2-JNKAR1EV-Clover FRET reporter provide a real-time
579 readout of JNK activity. The mRuby2 image (left) indicates reporter expression and FRET image
580 (right) indicates JNK activity, which is high in the cytoplasmic compartment. The look up table
581 (LUT) shows FRET ratios (F_c) from 0 to 1. **B.** mRuby2-JNKAR1EV-Clover FRET reporter activity
582 from hippocampal neuron dendrites increases following JNK activation following anisomycin (10
583 μ M) treatment. **C.** Normalized FRET (N-FRET) shows that JNK is activated in dendrites and spines
584 40 min following anisomycin (10 μ M). Mean data +/- S.E.M. are shown. *p*-values are from
585 Student's t-test. **Extended Data Figure 2-1** shows mRuby2-JNKAR1EV-Clover FRET has

586 improved dynamic range compared to YPET-JNKAR1EV-CFP. **D.** Representative image of
587 mRuby2-JNKAR1EV-Clover FRET in dendritic spines. **E.** FRET images from live cell analysis
588 indicate Flag-JBD inhibits JNK, as does LOV2-JBD following photo-stimulation for 30s with 0.4
589 mW of 458 nm laser. **F.** Corrected FRET (F_c) from multiple experiments as described in E.
590 Measurements were from 5 regions of interest per cell, from 4 cells from at least 2 experimental
591 repeats. Mean data \pm S.E.M. are shown. Adjusted p -values are shown from repeated measures
592 one-way ANOVA with Bonferroni correction. **Extended Data Figure 2-2** shows independent
593 readout of JNK activity changed due to excitation of the FRET probe with 488 nm laser. **G.** GFP-
594 actin displacement is shown in arithmetic difference projections (diff. proj.) depicting summed
595 GFP-actin displacements from 11 min imaging. Darker pixels represent higher motility. Scale bar =
596 3 μ m. **H.** Calculated motility index from several recordings as described in G. Flag-JBD and
597 LOV2-JBD *lit-state* mutants significantly reduce spine motility. Mean data \pm S.E.M. are shown.
598 Adjusted p -values are shown from repeated measures one-way ANOVA with Bonferroni correction
599 **I.** The minimal illumination required to photo-activate LOV2-JBD is shown. Motility changes from
600 neurons expressing mCherry-actin plus LOV2-JBD and exposed to increasing 458 nm irradiance
601 are shown. 0.4 mW (achieved using 3% laser power on Zeiss LSM-780) was the minimum
602 irradiance needed to elicit a maximal response. Motility was calculated from 4-6 spines per cell and
603 2-3 cells per condition from at least 2 experimental repeats.

604

605 **Figure 3. Photo-activation of the LOV2-JBD inhibitor rapidly reduces actin motility in the**

606 **peripheral domain of the spine. A.** Time-lapse sequences from 16 d hippocampal neurons

607 expressing mCherry-actin and LOV2-JBD variants. Regions of interest (blue squares)

608 encompassing spine-heads were photo-stimulated for 1 s at 36 s using 0.4 mW of 458 nm light.

609 Spine-head motility was reduced following light only in cells expressing LOV2-JBD. Additional

610 examples are in **Extended Data Figure 3-1A. B** shows arithmetic difference projections of

611 mCherry-actin before (pre) and after (post) 458 nm illumination of the spine (blue box). LOV2-JBD
612 immobilized mCherry-actin in photoactivated spines only. Dendritic shaft mCherry-actin was
613 unchanged. **C.** Quantitative data on mCherry actin motility. Spine numbers are indicated on the
614 bars. **D.** mCherry-actin motility changes are plotted according to spine head diameter:neck length
615 ratio. Data from spines with head diameter:neck length ratios corresponding to ‘mushroom’ spines
616 is in **Extended Data Figure 3-1 B.** **E.** Time-lapse of spine-head mCherry-actin motility shows
617 LOV2-JBD immobilizes actin motility within 6 s of photo-activation. **F.** Light alone does not alter
618 actin dynamics. For E-F, ≥ 4 spines were measured per cell. **G.** Color-coded time projections
619 provide spatial information on mCherry-actin motility over 90 s recording. Photo-activation is at 0
620 s. Images are acquired at 6 s intervals and coded with a unique hue (LUT). Mixed color (white-ish)
621 indicates continued motility over time. Blue indicates no further movement after that timepoint.
622 LOV2-JBD-expressing neurons display reduced motility following light. **H.** Higher resolution
623 maximum projections of temporally color-coded dendritic spines are shown from 10 s time-lapses
624 acquired at 1 s intervals. These show mCherry-actin is immobilized in the spine periphery.
625 Additional examples with actin footprints and movies generated from the time lapses are in
626 **Extended Data Figure 3-1 C-E.** **I.** The effect of latrunculin and phalloidin on dendritic spine
627 motility were tested. Arithmetic projection images before and after 458 nm light indicate effect on
628 actin dynamics. **J.** Quantitative data from I indicates that latrunculin reduces actin motility.
629 Measurements are from ≥ 10 cells and multiple spines from separate experiments. **K.** Temporal
630 color coding of spines from neurons treated with latrunculin or phalloidin are shown.

631

632 **Figure 4. Corticosterone activates JNK and induces SEP-GluR2 removal and spine**

633 **regression.** **A.** Time-lapse recording of JNK activity in dendritic spines after corticosterone
634 (CORT) application. Normalized Fc FRET is from 6 cells and ≥ 4 spines per cell. **B.** Representative
635 FRET ratio images from mRuby2-JNKAR1EV-Clover expressing cells. **C.** Representative images

636 of time-lapse sequences (D and E) from 16 d hippocampal neurons expressing mCherry-actin
637 (magenta), SEP-GluR2 (green) and LOV2-JBD. Cells were treated with CORT (100 nM) at 0 min
638 and LOV2-JBD was photo-activated using 458 nm 1s light pulses (using 3% laser power, LSM-880
639 Airyscan) applied to r.o.i. (blue boxes) at 3 min intervals where indicated (+458 nm), or in lower
640 panels, after a 20 min delay. SEP-GluR2 was imaged using the 488 nm laser (0.8% laser power with
641 LSM-880 Airyscan), to minimize cross-activation of LOV2-JBD. **D.** Quantitative data on cell
642 surface SEP-GluR2 fluorescence is from 8 experiments as depicted in C. **E.** Estimated spine-head
643 volume is normalized to baseline volume, averaged over 3 min before treatment. **Extended Data**
644 **Figure 4-1** shows experiments repeated as in Figure 4C, D, E with CORT treatment using YFP as
645 an inert filler instead of mCherry-Actin. Quantitative data is calculated from 8 experiments.
646 Adjusted *p*-values comparing full timelines are from repeated measures one-way ANOVA with
647 Bonferroni correction.

648

649 **Figure 5. NMDA activates spine-head JNK and induces retraction.**

650 **A.** Time lapse of JNK activity from mRuby2-JNKAR-1EV-Clover FRET reporter. Region of
651 interest FRET (Fc) was measured from spines of 16 d hippocampal neurons before and after
652 NMDA (20 μ M). **B.** Representative FRET images before and after NMDA. **C.** The estimated spine-
653 head volume from neurons expressing mCherry-actin and LOV2-JBD before (-3 min) or after
654 treatment with NMDA are shown. Continuous photo-activation of LOV2-JBD was achieved using
655 1s pulses of 458 nm laser (3% power) at 3 min intervals. LOV2-JBD photo-activation prevented
656 NMDA-induced spine retraction. **D.** The experimental setup for anisomycin (10 μ M) treatment and
657 photo-activation timeline is shown. The “*” indicates time point at which JNK was activated. **E.**
658 Neurons were treated with or without anisomycin and spine volume measured at 45 min (as
659 described in D). Anisomycin induced spine retraction which was prevented by LOV2-JBD photo-
660 activation. **F.** Mean data +/- S.E.M. from 20-24 spines/treatment is shown. Adjusted *p*-values

661 comparing full timelines are shown from repeated measures one-way ANOVA with Bonferroni
662 correction.

663

664 **Figure 6. Ketamine inhibits JNK and prevents spine regression when given prophylactically,**
665 **whereas JNK inhibition provides more robust rescue even 2h after CORT.**

666 **A.** We tested the effect of ketamine (10 μ M) on JNK activity in 16 d hippocampal neurons using the
667 mRuby2-JNKAR1EV-Clover FRET reporter. FC FRET responses in spine-head ROIs are from 7
668 separate experiments plotted individually. *p*-values are shown from repeated measures one-way
669 ANOVA with Bonferroni correction. Ketamine inhibited JNK activity, visible by 10 min post-
670 addition. **B.** The effect was long lasting. Representative FRET ratio images show mRuby2-
671 JNKAR1EV-Clover JNK activity reporter FRET before and 2 h following ketamine. **C.**
672 Representative images of 16 d hippocampal neurons expressing mCherry-actin (magenta), SEP-
673 GluR2 (green) +/- LOV2-JBD. Cells were stimulated with 100 nM corticosterone (CORT) or 10
674 μ M ketamine (KET), as indicated. Blue boxes indicate r.o.i. where 458 nm light was applied (1 s
675 pulses at 3 min intervals) to photo-activate LOV2-JBD. **D.** Estimated spine volume changes were
676 calculated from multiple images as shown in C, normalized to baseline. 8 cells, 4 spines per cell
677 were used. **E.** Quantitative data of cell surface SEP-GluR2 (SEP-GluR2 fluorescence/mCherry-actin
678 fluorescence) is shown from the same cells as in D. Measurements are from 8 experiments. **F.**
679 Dendritic spine volume changes were calculated from cells pretreated with 10 μ M ketamine or 10
680 μ M DJNKI-1 (to inhibit JNK) 2 h before addition of CORT (100 nM) for 2 h. **G.** Cell surface SEP-
681 GluR2 levels (SEP-GluR2 fluorescence/mCherry-actin fluorescence) was measured from the same
682 cells. **H.** Estimated spine volume changes were from \geq 8 experiments. 16 d neurons were treated
683 with CORT (100 nM) for 2 h followed by KET (10 μ M) or DJNKI-1 (10 μ M). Estimated spine
684 volume was measured and volume at 4 h was expressed relative to control. **I.** Cell surface GluR2
685 levels (SEP-GluR2/mCherry-actin) were calculated from the same cells. Mean data +/- S.E.M. are

686 shown. Adjusted p -values are shown from repeated measures one-way ANOVA with Bonferroni
687 correction.

688

689 **Extended Data Figure 1-1. Testing functionality of LOV2-JBD tools in neurons expressing**

690 **mCherry-NES-Jun as a JNK activity reporter. A.** Fluorescent micrographs from 16-day

691 hippocampal neurons expressing the mCherry-NES-Jun reporter in the presence, or absence

692 (control) of the *dark state* and *lit state* mutants of LOV2-JBD as indicated. Micrographs show ratio

693 images of phospho-Ser63-c-Jun (P-Jun)/mCherry-NES-Jun (mCherry) fluorescence. Scale bar = 15

694 μm . **B.** JNK activity (from multiple experiments as shown in A) is the ratio of phosphorylated c-Jun

695 normalized to mCherry-NES-Jun reporter expression. The “*lit-state*” mutant of LOV2-JBD reduced

696 JNK activity even without photo-stimulation. The “*dark-state*” mutant did not significantly alter

697 JNK activity even in the presence of light. Mean data +/- S.E.M. are shown. *p*-values are shown

698 from repeated measures one-way ANOVA and are indicated above the histogram bars. Total

699 number of cells analyzed from at least two experimental repeats are indicated on the bars.

700

701 **Extended Data Figure 2-1. mRuby2/Clover pairing improves JNK FRET reporter sensitivity.**

702 **A.** The sensitivity of FRET response was compared using the EYFP-JNKAR1EV-CFP FRET

703 reporter and the newly generated mRuby2-JNKAR1EV-Clover reporter. Reporter activity was

704 measured in 16 day hippocampal neurons treated with anisomycin (10 μM). **B.** Normalized FRET

705 (N-FRET) was measured from multiple cells expressing both reporters. mRuby2-JNKAR1EV-

706 Clover provided improved dynamic range compared to EYFP-JNKAR1EV-CFP (dendrite,

707 $p=0.000167$). Measurements were from 5 regions per cell and 4 cells per experiment on two

708 separate experiments. Mean data +/- S.E.M. are shown.

709

710 **Extended Data Figure 2-2. 488 nm irradiation in neurons expressing LOV2-JBD partially**

711 **inhibits JNK.** Fluorescent micrographs from 16-day hippocampal neurons expressing mCherry-

712 NES-Jun+LOV2-JBD in the presence, or absence of 488 nm irradiation mimicking Clover/FRET

713 channel excitation (0.4 mW). Micrographs show ratio images of phospho-Ser63-c-Jun (P-
714 Jun)/mCherry-NES-Jun (mCherry) fluorescence. Scale bar = 15 μ m. **B.** JNK activity (from multiple
715 experiments as shown in A) is the ratio of phosphorylated c-Jun normalized to mCherry-NES-Jun
716 reporter expression. Mean data +/- S.E.M. are shown, *p*-value is obtained by Student's t-test.

717

718 **Extended Data Figure 3-1. Photo-stimulation of LOV2-JBD in dendritic spines rapidly**
719 **immobilizes spine-head actin in the peripheral domain. A.** Time-lapse sequences from 16 day
720 hippocampal neurons expressing mCherry-actin and LOV2-JBD variants as indicated. Cells were
721 stimulated for 1 s with 0.4 mW of 458 nm light. **B.** The effect on spine motility of LOV2-JBD
722 photo-activation in mushroom spines (head diameter:neck length ratio >3) is shown. Spine motility
723 is measured from arithmetic difference projection ratios (motility after light/motility before light).
724 Optical stimulation of mushroom spines did not alter mCherry-actin motility in spines even when
725 laser power was increased to compensate for larger spine-head volume. At least 6 spines from 4
726 experimental repeats were measured for each condition. Mean data +/- S.E.M. are shown **C.** High
727 resolution maximum projections show temporally color-coded dendritic spines from 10 s time-lapse
728 from 3D recordings using Airyscan mode, at 1 s intervals. **D.** Footprints of time lapse sequences are
729 shown for color-coded time projections from cells expressing mCherry-Actin with or without
730 LOV2-JBD for spines shown in C. **E.** Movies generated from 3D Airyscan recordings (1s interval)
731 of dendritic spines of a cell expressing mCherry-Actin with LOV2-JBD as shown in **Movie 1.mp4**:
732 Time lapse movie 0 s to 120s, blue circle depicts ROI of 458 nm illumination. **Movie 2.mp4**:
733 Volumetric temporal color coding of a dendritic spine generated from 48s to 58s with 1 s 458nm
734 illumination at 48s.

735

736 **Extended Data Figure 4-1. Optogenetic inhibition of JNK recovers regressed spines and SEP-**
737 **GluR2 induced by corticosterone. A.** Time-lapse sequences from 16-day hippocampal neurons

738 expressing eYFP-C1 (magenta), SEP-GluR2 (green) and LOV2-JBD. Cells were treated with 100
739 nM CORT at 0 min. 458 nm light pulses were applied every 3 min where indicated (+458 nm). **B.**
740 Quantitative data shows spine-head volume changes relative to baseline, calculated from 6
741 experiments. **C.** Quantitative data shows plasma membrane SEP-GluR2 fluorescence normalized to
742 YFP. Data is from 6 experiments as depicted in C. Adjusted *p*-values (written on the graph) are
743 from comparisons of full timelines from multiple experiments using repeated measures one-way
744 ANOVA with Bonferroni correction. Endpoint averages are also shown.

745

746 **Movie 1. 4D time-lapse showing the effect of photo-activation of LOV2-JBD on spine**
747 **dynamics.** Movie generated from 3D Airyscan recording (1s interval) of a dendritic spine from a
748 cell expressing mCherry-Actin with LOV2-JBD, blue circle depicts ROI of 458 nm illumination. A
749 decrease in spine head dynamics is visible moments after photoactivation of LOV2-JBD.

750

751 **Movie 2. Volumetric temporal color coding of a dendritic spine after photo-activation of**
752 **LOV2-JBD.** Reconstruction of **Movie 1**, generated from 48s to 58s with 1 s 458nm illumination at
753 48s. Note the halted actin dynamics following photoactivation of LOV2-JBD (blue).

754

755 REFERENCES

756

757 Attardo A, Fitzgerald JE, Schnitzer MJ (2015) Impermanence of dendritic spines in live adult CA1
758 hippocampus. *Nature* 523:592-596.

759 Basu S, Saha PK, Roszkowska M, Magnowska M, Baczynska E, Das N, Plewczynski D,
760 Wlodarczyk J (2018) Quantitative 3-D morphometric analysis of individual dendritic spines.
761 *Sci Rep* 8:3545.

762 Bennett S, Thomas AJ (2014) Depression and dementia: cause, consequence or coincidence?
763 *Maturitas* 79:184-190.

764 Berry KP, Nedivi E (2017) Spine Dynamics: Are They All the Same? *Neuron* 96:43-55.

765 Bertling E, Englund J, Minkeviciene R, Koskinen M, Segerstråle M, Castrén E, Taira T, Hotulainen
766 P (2016) Actin Tyrosine-53-Phosphorylation in Neuronal Maturation and Synaptic
767 Plasticity. *J Neurosci* 36:5299-5313.

768 Bevilaqua LR, Kerr DS, Medina JH, Izquierdo I, Cammarota M (2003) Inhibition of hippocampal
769 Jun N-terminal kinase enhances short-term memory but blocks long-term memory formation
770 and retrieval of an inhibitory avoidance task. *Eur J Neurosci* 17:897-902.

771 Björkblom B, Padzik A, Mohammad H, Westerlund N, Komulainen E, Hollos P, Parviainen L,
772 Papageorgiou AC, Iljin K, Kallioniemi O, Kallajoki M, Courtney MJ, Magard M, James P,
773 Coffey ET (2012) c-Jun N-terminal kinase phosphorylation of MARCKSL1 determines
774 actin stability. *Mol Cell Biol* 32:3513-3526.

775 Björkblom B, Ostman N, Hongisto V, Komarovski V, Filén JJ, Nyman TA, Kallunki T, Courtney
776 MJ, Coffey ET (2005) Constitutively active cytoplasmic c-Jun N-terminal kinase 1 is a
777 dominant regulator of dendritic architecture: role of microtubule-associated protein 2 as an
778 effector. *J Neurosci* 25:6350-6361.

- 779 Bonny C, Oberson A, Negri S, Sauser C, Schorderet DF (2001) Cell-permeable peptide inhibitors
780 of JNK: novel blockers of beta-cell death. *Diabetes* 50:77-82.
- 781 Borsello T, Clarke PG, Hirt L, Vercelli A, Repici M, Schorderet DF, Bogousslavsky J, Bonny C
782 (2003) A peptide inhibitor of c-Jun N-terminal kinase protects against excitotoxicity and
783 cerebral ischemia. *Nat Med* 9:1180-1186.
- 784 Brecht S, Kirchhof R, Chromik A, Willeßen M, Nicolaus T, Raivich G, Wessig J, Waetzig V, Goetz
785 M, Claussen M, Pearse D, Kuan CY, Vaudano E, Behrens A, Wagner E, Flavell RA, Davis
786 RJ, Herdegen T (2005) Specific pathophysiological functions of JNK isoforms in the brain.
787 *Eur J Neurosci* 21:363-377.
- 788 Cano E, Hazzalin CA, Mahadevan LC (1994) Anisomycin-activated protein kinases p45 and p55
789 but not mitogen-activated protein kinases ERK-1 and -2 are implicated in the induction of c-
790 fos and c-jun. *Mol Cell Biol* 14:7352-7362.
- 791 Chen F, Madsen TM, Wegener G, Nyengaard JR (2009) Imipramine treatment increases the number
792 of hippocampal synapses and neurons in a genetic animal model of depression.
793 *Hippocampus* 20:1376-1384.
- 794 Cingolani LA, Goda Y (2008) Actin in action: the interplay between the actin cytoskeleton and
795 synaptic efficacy. *Nat Rev Neurosci* 9:344-356.
- 796 Cingolani LA, Thalhammer A, Yu LM, Catalano M, Ramos T, Colicos MA, Goda Y (2008)
797 Activity-dependent regulation of synaptic AMPA receptor composition and abundance by
798 beta3 integrins. *Neuron* 58:749-762.
- 799 Coffey ET (2014) Nuclear and cytosolic JNK signalling in neurons. *Nat Rev Neurosci* 15:285-299.
- 800 Coffey ET, Hongisto V, Dickens M, Davis RJ, Courtney MJ (2000) Dual roles for c-Jun N-terminal
801 kinase in developmental and stress responses in cerebellar granule neurons. *J Neurosci*
802 20:7602-7613.

- 803 Costello DA, Herron CE (2004) The role of c-Jun N-terminal kinase in the A beta-mediated
804 impairment of LTP and regulation of synaptic transmission in the hippocampus.
805 *Neuropharmacology* 46:655-662.
- 806 Curran BP, Murray HJ, O'Connor JJ (2003) A role for c-Jun N-terminal kinase in the inhibition of
807 long-term potentiation by interleukin-1beta and long-term depression in the rat dentate gyrus
808 in vitro. *Neuroscience* 118:347-357.
- 809 Duman CH, Duman RS (2015) Spine synapse remodeling in the pathophysiology and treatment of
810 depression. *Neurosci Lett* 601:20-29.
- 811 Duman RS (2009) Neuronal damage and protection in the pathophysiology and treatment of
812 psychiatric illness: stress and depression. *Dialogues Clin Neurosci* 11:239-255.
- 813 Duman RS, Aghajanian GK (2012) Synaptic dysfunction in depression: potential therapeutic
814 targets. *Science* 338:68-72.
- 815 Duman RS, Li N, Liu RJ, Duric V, Aghajanian G (2011) Signaling pathways underlying the rapid
816 antidepressant actions of ketamine. *Neuropharmacology* 62:35-41.
- 817 Engert F, Bonhoeffer T (1999) Dendritic spine changes associated with hippocampal long-term
818 synaptic plasticity. *Nature* 399:66-70.
- 819 Fischer M, Kaech S, Knutti D, Matus A (1998) Rapid actin-based plasticity in dendritic spines.
820 *Neuron* 20:847-854.
- 821 Fischer M, Kaech S, Wagner U, Brinkhaus H, Matus A (2000) Glutamate receptors regulate actin-
822 based plasticity in dendritic spines. *Nat Neurosci* 3:887-894.
- 823 Ge S, Yang Ch, Hsu Ks, Ming Gl, Song H (2007) A Critical Period for Enhanced Synaptic
824 Plasticity in Newly Generated Neurons of the Adult Brain. *Neuron* 54:559-566.
- 825 Hajszan T, Dow A, Warner-Schmidt JL, Szigeti-Buck K, Sallam NL, Parducz A, Leranath C, Duman
826 RS (2009) Remodeling of hippocampal spine synapses in the rat learned helplessness model
827 of depression. *Biol Psychiatry* 65:392-400.

- 828 Halavaty AS, Moffat K (2007) N- and C-terminal flanking regions modulate light-induced signal
829 transduction in the LOV2 domain of the blue light sensor phototropin 1 from *Avena sativa*.
830 *Biochemistry* 46:14001-14009.
- 831 Hanley JG (2014) Actin-dependent mechanisms in AMPA receptor trafficking. *Front Cell Neurosci*
832 8:381.
- 833 Harper SM, Christie JM, Gardner KH (2004) Disruption of the LOV-Jalpha helix interaction
834 activates phototropin kinase activity. *Biochemistry* 43:16184-16192.
- 835 Heo YS, Kim SK, Seo CI, Kim YK, Sung BJ, Lee HS, Lee JI, Park SY, Kim JH, Hwang KY, Hyun
836 YL, Jeon YH, Ro S, Cho JM, Lee TG, Yang CH (2004) Structural basis for the selective
837 inhibition of JNK1 by the scaffolding protein JIP1 and SP600125. *EMBO J* 23:2185-2195.
- 838 Hollos P, Marchisella F, Coffey ET (2018) JNK Regulation of Depression and Anxiety. *Brain Plast*
839 3:145-155.
- 840 Holtmaat A, Caroni P (2016) Functional and structural underpinnings of neuronal assembly
841 formation in learning. *Nat Neurosci* 19:1553-1562.
- 842 Holtmaat A, De Paola V, Wilbrecht L, Knott GW (2008) Imaging of experience-dependent
843 structural plasticity in the mouse neocortex in vivo. *Behav Brain Res* 192:20-25.
- 844 Honkura N, Matsuzaki M, Noguchi J, Ellis-Davies GC, Kasai H (2008) The subspine organization
845 of actin fibers regulates the structure and plasticity of dendritic spines. *Neuron* 57:719-729.
- 846 Hruska M, Henderson N, Le Marchand SJ, Jafri H, Dalva MB (2018) Synaptic nanomodules
847 underlie the organization and plasticity of spine synapses. *Nat Neurosci* 21:671-682.
- 848 Huganir RL, Nicoll RA (2013) AMPARs and synaptic plasticity: the last 25 years. *Neuron* 80:704-
849 717.
- 850 Kasai H, Fukuda M, Watanabe S, Hayashi-Takagi A, Noguchi J (2010) Structural dynamics of
851 dendritic spines in memory and cognition. *Trends Neurosci* 33:121-129.

- 852 Kessels HW, Kopec CD, Klein ME, Malinow R (2009) Roles of stargazin and phosphorylation in
853 the control of AMPA receptor subcellular distribution. *Nat Neurosci* 12:888-896.
- 854 Komatsu N, Aoki K, Yamada M, Yukinaga H, Fujita Y, Kamioka Y, Matsuda M (2011)
855 Development of an optimized backbone of FRET biosensors for kinases and GTPases. *Mol*
856 *Biol Cell* 22:4647-4656.
- 857 Komulainen E, Zdrojewska J, Freemantle E, Mohammad H, Kuleskaya N, Deshpande P,
858 Marchisella F, Mysore R, Hollos P, Michelsen KA, Mågard M, Rauvala H, James P, Coffey
859 ET (2014) JNK1 controls dendritic field size in L2/3 and L5 of the motor cortex, constrains
860 soma size, and influences fine motor coordination. *Front Cell Neurosci* 8:272.
- 861 Kowalchuk C, Kanagasundaram P, Belsham DD, Hahn MK (2019) Antipsychotics differentially
862 regulate insulin, energy sensing, and inflammation pathways in hypothalamic rat neurons.
863 *Psychoneuroendocrinology* 104:42-48.
- 864 Krieger E, Joo K, Lee J, Raman S, Thompson J, Tyka M, Baker D, Karplus K (2009) Improving
865 physical realism, stereochemistry, and side-chain accuracy in homology modeling: Four
866 approaches that performed well in CASP8. *Proteins* 77 Suppl 9:114-122.
- 867 Kunde SA, Rademacher N, Tzschach A, Wiedersberg E, Ullmann R, Kalscheuer VM, Shoichet SA
868 (2013) Characterisation of de novo MAPK10/JNK3 truncation mutations associated with
869 cognitive disorders in two unrelated patients. *Hum Genet* 132:461-471.
- 870 Kyriakis JM, Avruch J (2012) Mammalian MAPK signal transduction pathways activated by stress
871 and inflammation: a 10-year update. *Physiol Rev* 92:689-737.
- 872 Lee HK, Kameyama K, Huganir RL, Bear MF (1998) NMDA induces long-term synaptic
873 depression and dephosphorylation of the GluR1 subunit of AMPA receptors in
874 hippocampus. *Neuron* 21:1151-1162.
- 875 Lendvai B, Stern EA, Chen B, Svoboda K (2000) Experience-dependent plasticity of dendritic
876 spines in the developing rat barrel cortex in vivo. *Nature* 404:876-881.

- 877 Li XM, Li CC, Yu SS, Chen JT, Sabapathy K, Ruan DY (2007) JNK1 contributes to metabotropic
878 glutamate receptor-dependent long-term depression and short-term synaptic plasticity in the
879 mice area hippocampal CA1. *Eur J Neurosci* 25:391-396.
- 880 Liston C, Gan WB (2011) Glucocorticoids are critical regulators of dendritic spine development and
881 plasticity in vivo. *Proc Natl Acad Sci U S A* 108:16074-16079.
- 882 Lüscher C, Malenka RC (2012) NMDA receptor-dependent long-term potentiation and long-term
883 depression (LTP/LTD). *Cold Spring Harb Perspect Biol* 4.
- 884 Malhi GS, Mann JJ (2018) Depression. *Lancet* 392:2299-2312.
- 885 Matsuzaki M, Honkura N, Ellis-Davies GC, Kasai H (2004) Structural basis of long-term
886 potentiation in single dendritic spines. *Nature* 429:761-766.
- 887 Matsuzaki M, Ellis-Davies GC, Nemoto T, Miyashita Y, Iino M, Kasai H (2001) Dendritic spine
888 geometry is critical for AMPA receptor expression in hippocampal CA1 pyramidal neurons.
889 *Nat Neurosci* 4:1086-1092.
- 890 McAvoy K, Russo C, Kim S, Rankin G, Sahay A (2015) Fluoxetine induces input-specific
891 hippocampal dendritic spine remodeling along the septotemporal axis in adulthood and
892 middle age. *Hippocampus*.
- 893 McGuire JL, Depasquale EA, Funk AJ, O'Donovan SM, Hasselfeld K, Marwaha S, Hammond JH,
894 Hartounian V, Meador-Woodruff JH, Meller J, McCullumsmith RE (2017) Abnormalities of
895 signal transduction networks in chronic schizophrenia. *NPJ Schizophr* 3:30.
- 896 Melero-Fernandez de Mera RM, Li LL, Popinigis A, Cisek K, Tuittila M, Yadav L, Serva A,
897 Courtney MJ (2017) A simple optogenetic MAPK inhibitor design reveals resonance
898 between transcription-regulating circuitry and temporally-encoded inputs. *Nat Commun*
899 8:15017.
- 900 Michelsen KA, van den Hove DL, Schmitz C, Segers O, Prickaerts J, Steinbusch HW (2007)
901 Prenatal stress and subsequent exposure to chronic mild stress influence dendritic spine
902 density and morphology in the rat medial prefrontal cortex. *BMC Neurosci* 8:107.

- 903 Moda-Sava RN, Murdock MH, Parekh PK, Fetcho RN, Huang BS, Huynh TN, Witztum J, Shaver
904 DC, Rosenthal DL, Alway EJ, Lopez K, Meng Y, Nellissen L, Grosenick L, Milner TA,
905 Deisseroth K, Bito H, Kasai H, Liston C (2019) Sustained rescue of prefrontal circuit
906 dysfunction by antidepressant-induced spine formation. *Science* 364.
- 907 Mohammad H, Marchisella F, Ortega-Martinez S, Hollos P, Eerola K, Komulainen E, Kuleshkaya
908 N, Freemantle E, Fagerholm V, Savontous E, Rauvala H, Peterson BD, van Praag H, Coffey
909 ET (2016) JNK1 controls adult hippocampal neurogenesis and imposes cell-autonomous
910 control of anxiety behaviour from the neurogenic niche. *Mol Psychiatry*.
- 911 Murase S, Lantz CL, Kim E, Gupta N, Higgins R, Stopfer M, Hoffman DA, Quinlan EM (2016)
912 Matrix Metalloproteinase-9 Regulates Neuronal Circuit Development and Excitability. *Mol*
913 *Neurobiol* 53:3477-3493.
- 914 Musazzi L, Racagni G, Popoli M (2011) Stress, glucocorticoids and glutamate release: effects of
915 antidepressant drugs. *Neurochem Int* 59:138-149.
- 916 Musazzi L, Treccani G, Popoli M (2015) Functional and structural remodeling of glutamate
917 synapses in prefrontal and frontal cortex induced by behavioral stress. *Front Psychiatry* 6:60.
- 918 Musazzi L, Tornese P, Sala N, Popoli M (2017) Acute or Chronic? A Stressful Question. *Trends*
919 *Neurosci* 40:525-535.
- 920 Musazzi L, Tornese P, Sala N, Popoli M (2018) What Acute Stress Protocols Can Tell Us About
921 PTSD and Stress-Related Neuropsychiatric Disorders. *Front Pharmacol* 9:758.
- 922 Musazzi L, Milanese M, Farisello P, Zappettini S, Tardito D, Barbiero VS, Bonifacino T, Mallei A,
923 Baldelli P, Racagni G, Raiteri M, Benfenati F, Bonanno G, Popoli M (2010) Acute stress
924 increases depolarization-evoked glutamate release in the rat prefrontal/frontal cortex: the
925 dampening action of antidepressants. *PLoS One* 5:e8566.
- 926 Myers KR, Wang G, Sheng Y, Conger KK, Casanova JE, Zhu JJ (2012) Arf6-GEF BRAG1
927 regulates JNK-mediated synaptic removal of GluA1-containing AMPA receptors: a new
928 mechanism for nonsyndromic X-linked mental disorder. *J Neurosci* 32:11716-11726.

- 929 Nimchinsky EA, Sabatini BL, Svoboda K (2002) Structure and function of dendritic spines. *Annu*
930 *Rev Physiol* 64:313-353.
- 931 Noguchi J, Nagaoka A, Watanabe S, Ellis-Davies GC, Kitamura K, Kano M, Matsuzaki M, Kasai H
932 (2011) In vivo two-photon uncaging of glutamate revealing the structure-function
933 relationships of dendritic spines in the neocortex of adult mice. *J Physiol* 589:2447-2457.
- 934 Openshaw RL, Thomson DM, Thompson R, Penninger JM, Pratt JA, Morris BJ, Dawson N (2019a)
935 *Map2k7 Haploinsufficiency Induces Brain Imaging Endophenotypes and Behavioral*
936 *Phenotypes Relevant to Schizophrenia. Schizophr Bull.*
- 937 Openshaw RL, Kwon J, McColl A, Penninger JM, Cavanagh J, Pratt JA, Morris BJ (2019b) JNK
938 signalling mediates aspects of maternal immune activation: importance of maternal
939 genotype in relation to schizophrenia risk. *J Neuroinflammation* 16:18.
- 940 Passafaro M, Piëch V, Sheng M (2001) Subunit-specific temporal and spatial patterns of AMPA
941 receptor exocytosis in hippocampal neurons. *Nat Neurosci* 4:917-926.
- 942 Peter E, Dick B, Baeurle SA (2010) Mechanism of signal transduction of the LOV2-J α photosensor
943 from *Avena sativa*. *Nat Commun* 1:122.
- 944 Qi AQ, Qiu J, Xiao L, Chen YZ (2005) Rapid activation of JNK and p38 by glucocorticoids in
945 primary cultured hippocampal cells. *J Neurosci Res* 80:510-517.
- 946 Radley JJ, Anderson RM, Hamilton BA, Alcock JA, Romig-Martin SA (2013) Chronic stress-
947 induced alterations of dendritic spine subtypes predict functional decrements in an
948 hypothalamo-pituitary-adrenal-inhibitory prefrontal circuit. *J Neurosci* 33:14379-14391.
- 949 Rubio FJ, Ampuero E, Sandoval R, Toledo J, Pancetti F, Wyneken U (2013) Long-term fluoxetine
950 treatment induces input-specific LTP and LTD impairment and structural plasticity in the
951 CA1 hippocampal subfield. *Front Cell Neurosci* 7:66.
- 952 Saito SY (2009) Toxins affecting actin filaments and microtubules. *Prog Mol Subcell Biol* 46:187-
953 219.

- 954 Sali A, Blundell TL (1993) Comparative protein modelling by satisfaction of spatial restraints. *J*
955 *Mol Biol* 234:779-815.
- 956 Salomon M, Christie JM, Knieb E, Lempert U, Briggs WR (2000) Photochemical and mutational
957 analysis of the FMN-binding domains of the plant blue light receptor, phototropin.
958 *Biochemistry* 39:9401-9410.
- 959 Sanacora G, Treccani G, Popoli M (2012) Towards a glutamate hypothesis of depression: an
960 emerging frontier of neuropsychopharmacology for mood disorders. *Neuropharmacology*
961 62:63-77.
- 962 Sclip A, Tozzi A, Abaza A, Cardinetti D, Colombo I, Calabresi P, Salmona M, Welker E, Borsello
963 T (2014) c-Jun N-terminal kinase has a key role in Alzheimer disease synaptic dysfunction
964 in vivo. *Cell Death Dis* 5:e1019.
- 965 Seo J, Hong J, Lee SJ, Choi SY (2012) c-Jun N-terminal phosphorylation is essential for
966 hippocampal synaptic plasticity. *Neurosci Lett* 531:14-19.
- 967 Sherrin T, Blank T, Todorovic C (2011) c-Jun N-terminal kinases in memory and synaptic
968 plasticity. *Rev Neurosci* 22:403-410.
- 969 Sherrin T, Blank T, Hippel C, Rayner M, Davis RJ, Todorovic C (2010) Hippocampal c-Jun-N-
970 terminal kinases serve as negative regulators of associative learning. *J Neurosci* 30:13348-
971 13361.
- 972 Solas M, Gerenu G, Gil-Bea FJ, Ramírez MJ (2013) Mineralocorticoid receptor activation induces
973 insulin resistance through c-Jun N-terminal kinases in response to chronic corticosterone:
974 cognitive implications. *J Neuroendocrinol* 25:350-356.
- 975 Treccani G, Ardalan M, Chen F, Musazzi L, Popoli M, Wegener G, Nyengaard JR, Müller HK
976 (2019) S-Ketamine Reverses Hippocampal Dendritic Spine Deficits in Flinders Sensitive
977 Line Rats Within 1 h of Administration. *Mol Neurobiol*.
- 978 Treccani G, Musazzi L, Perego C, Milanese M, Nava N, Bonifacino T, Lamanna J, Malgaroli A,
979 Drago F, Racagni G, Nyengaard JR, Wegener G, Bonanno G, Popoli M (2014) Acute stress

- 980 rapidly increases the readily releasable pool of glutamate vesicles in prefrontal and frontal
981 cortex through non-genomic action of corticosterone. *Mol Psychiatry* 19:401.
- 982 Varidaki A, Mohammad, H., Coffey, E.T. (2016) *Molecular mechanisms of depression*, 1st Edition:
983 Elsevier.
- 984 Wallner B, Elofsson A (2005) All are not equal: a benchmark of different homology modeling
985 programs. *Protein Sci* 14:1315-1327.
- 986 Westerlund N, Zdrojewska J, Padzik A, Komulainen E, Björkblom B, Rannikko E, Tararuk T,
987 Garcia-Frigola C, Sandholm J, Nguyen L, Kallunki T, Courtney MJ, Coffey ET (2011)
988 Phosphorylation of SCG10/stathmin-2 determines multipolar stage exit and neuronal
989 migration rate. *Nat Neurosci* 14:305-313.
- 990 Weston CR, Davis RJ (2007) The JNK signal transduction pathway. *Curr Opin Cell Biol* 19:142-
991 149.
- 992 Winchester CL, Ohzeki H, Vouyiouklis DA, Thompson R, Penninger JM, Yamagami K, Norrie JD,
993 Hunter R, Pratt JA, Morris BJ (2012) Converging evidence that sequence variations in the
994 novel candidate gene MAP2K7 (MKK7) are functionally associated with schizophrenia.
995 *Hum Mol Genet* 21:4910-4921.
- 996 Wohleb ES, Terwilliger R, Duman CH, Duman RS (2018) Stress-Induced Neuronal Colony
997 Stimulating Factor 1 Provokes Microglia-Mediated Neuronal Remodeling and Depressive-
998 like Behavior. *Biol Psychiatry* 83:38-49.
- 999 Zayner JP, Sosnick TR (2014) Factors that control the chemistry of the LOV domain photocycle.
1000 *PLoS One* 9:e87074.
- 1001 Zhou Q, Homma KJ, Poo MM (2004) Shrinkage of dendritic spines associated with long-term
1002 depression of hippocampal synapses. *Neuron* 44:749-757.
1003

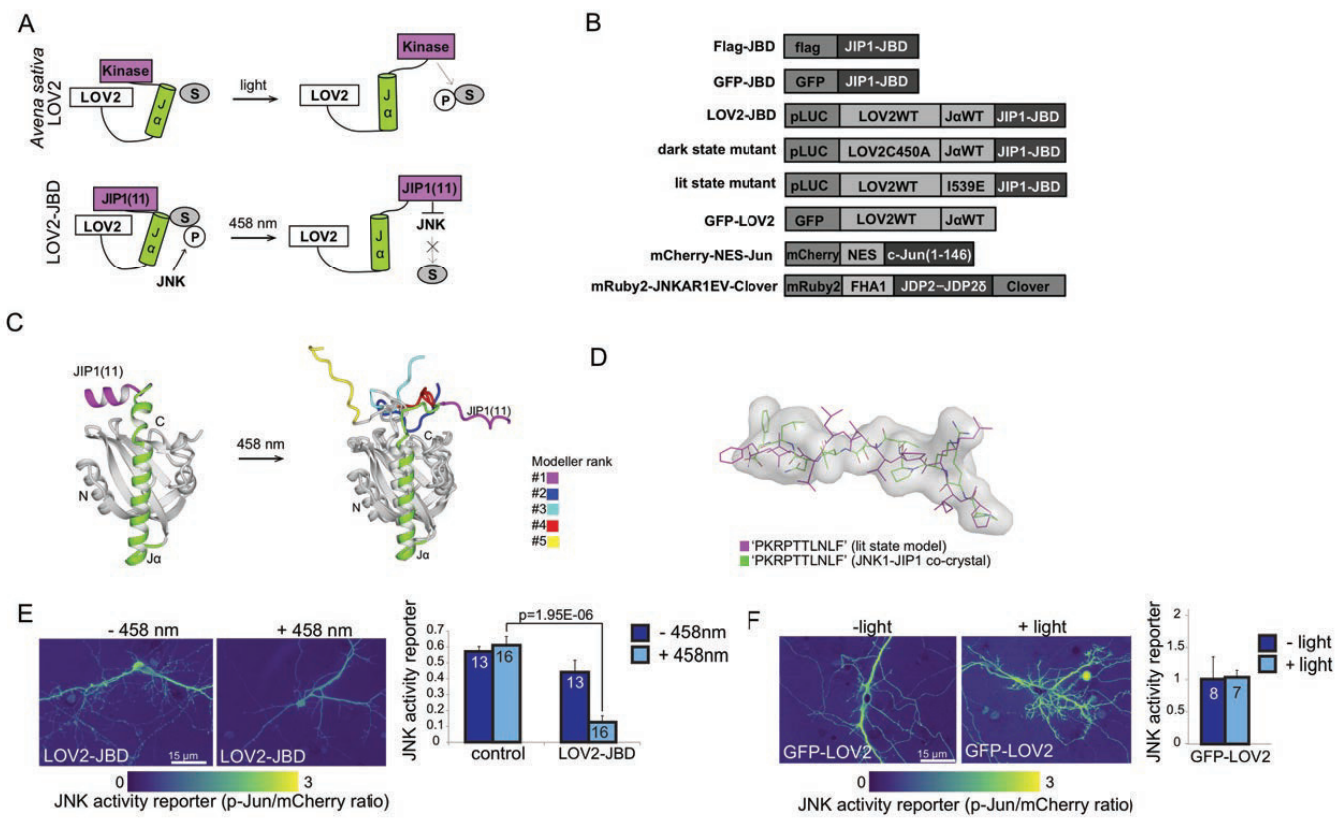


Figure 1

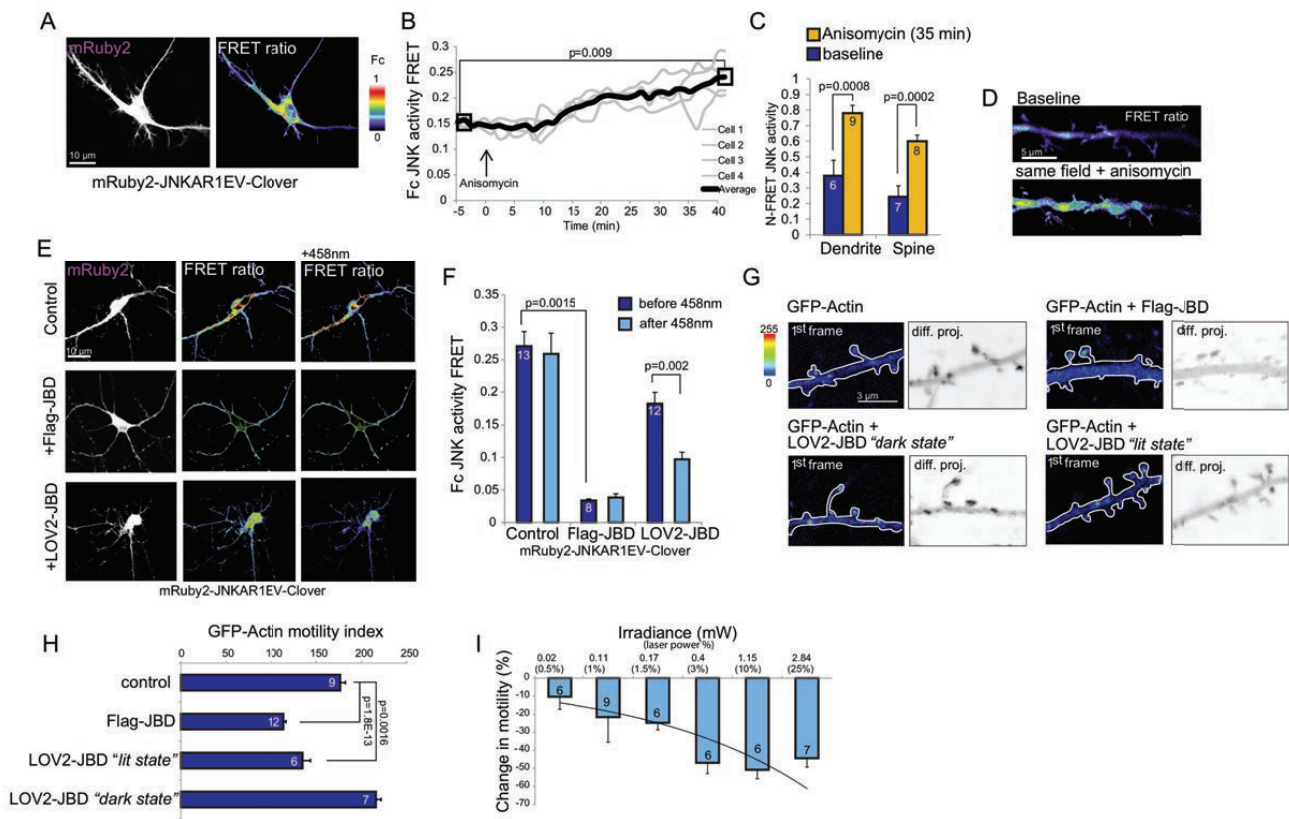


Figure 2

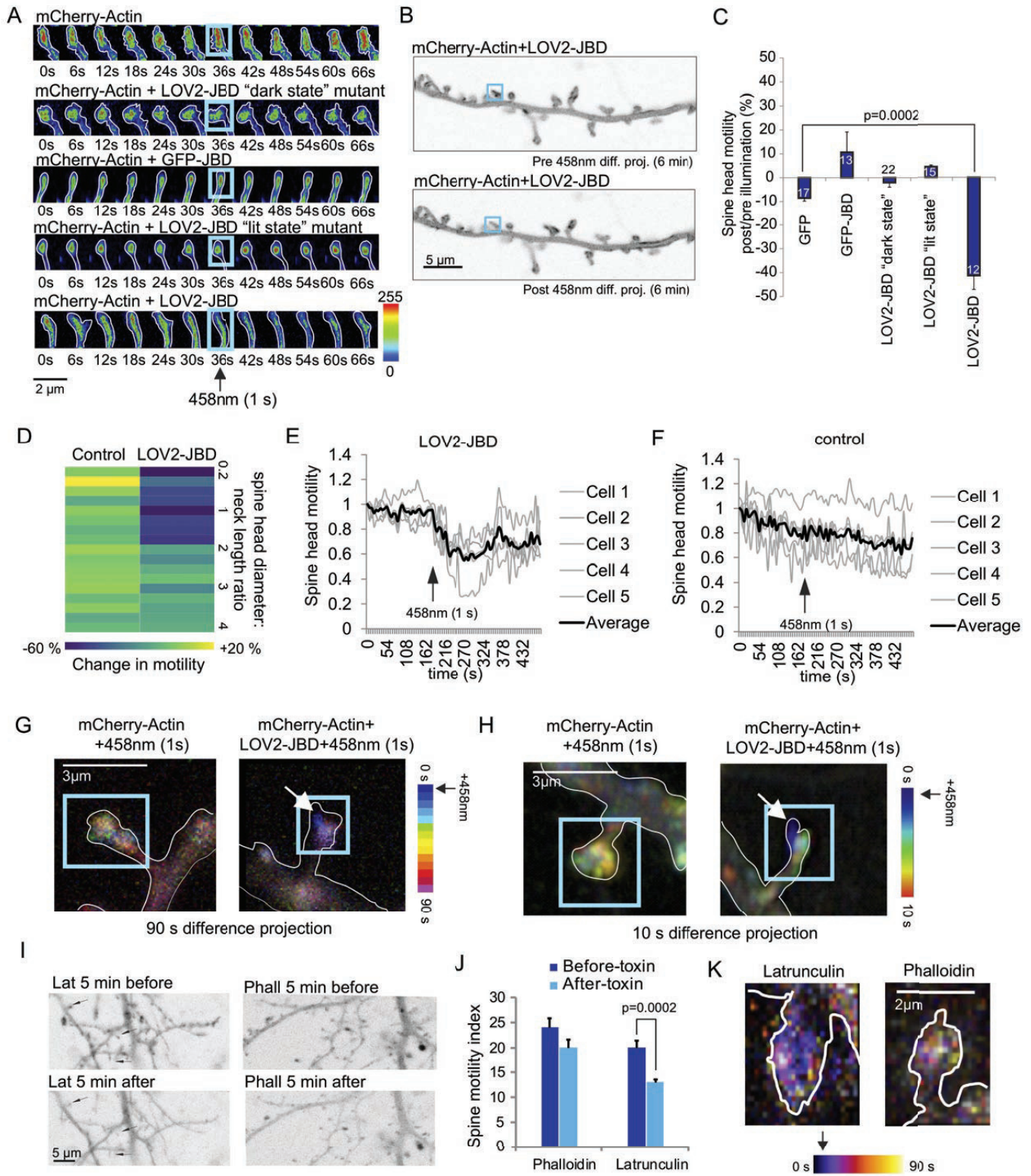


Figure 3

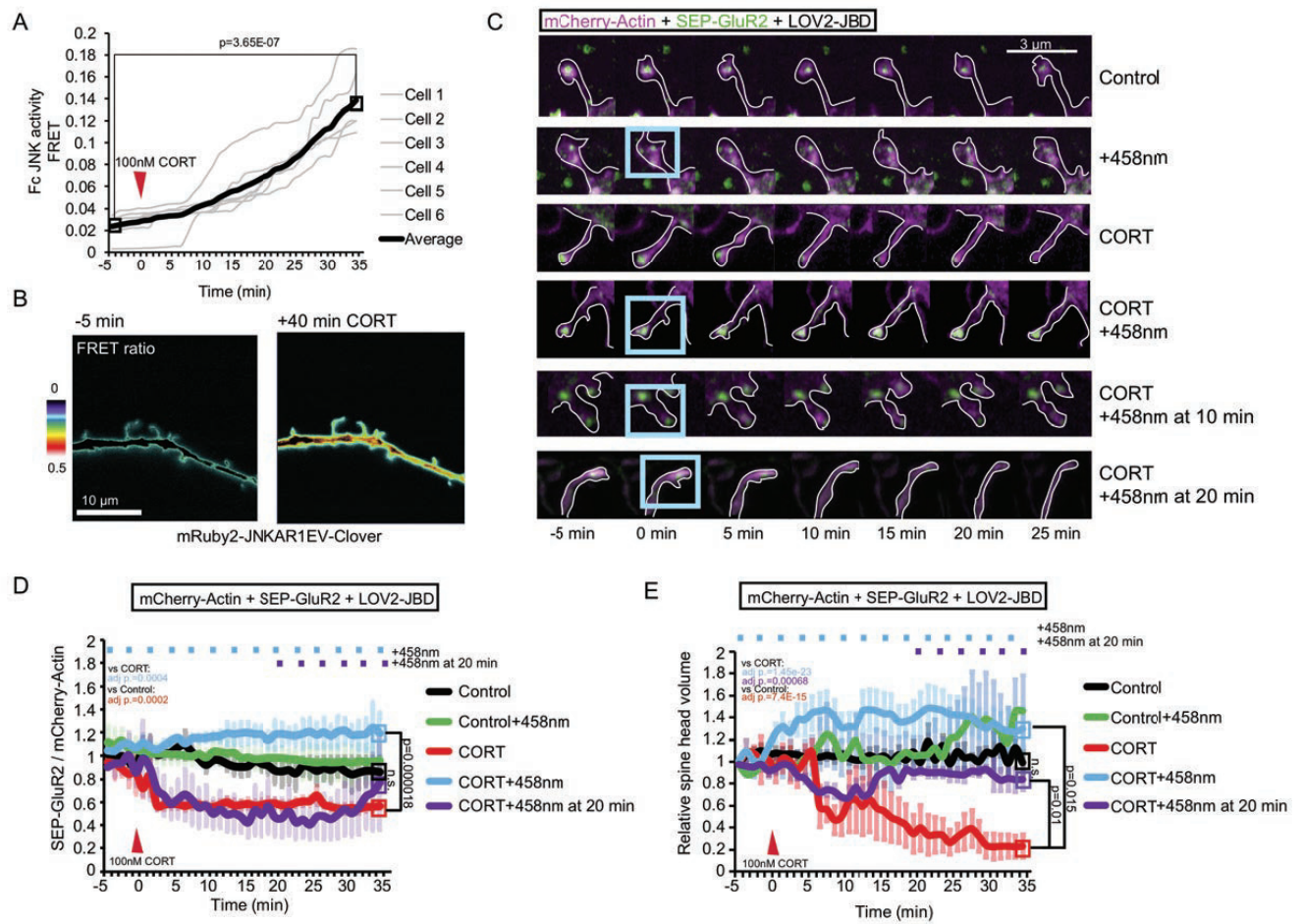


Figure 4

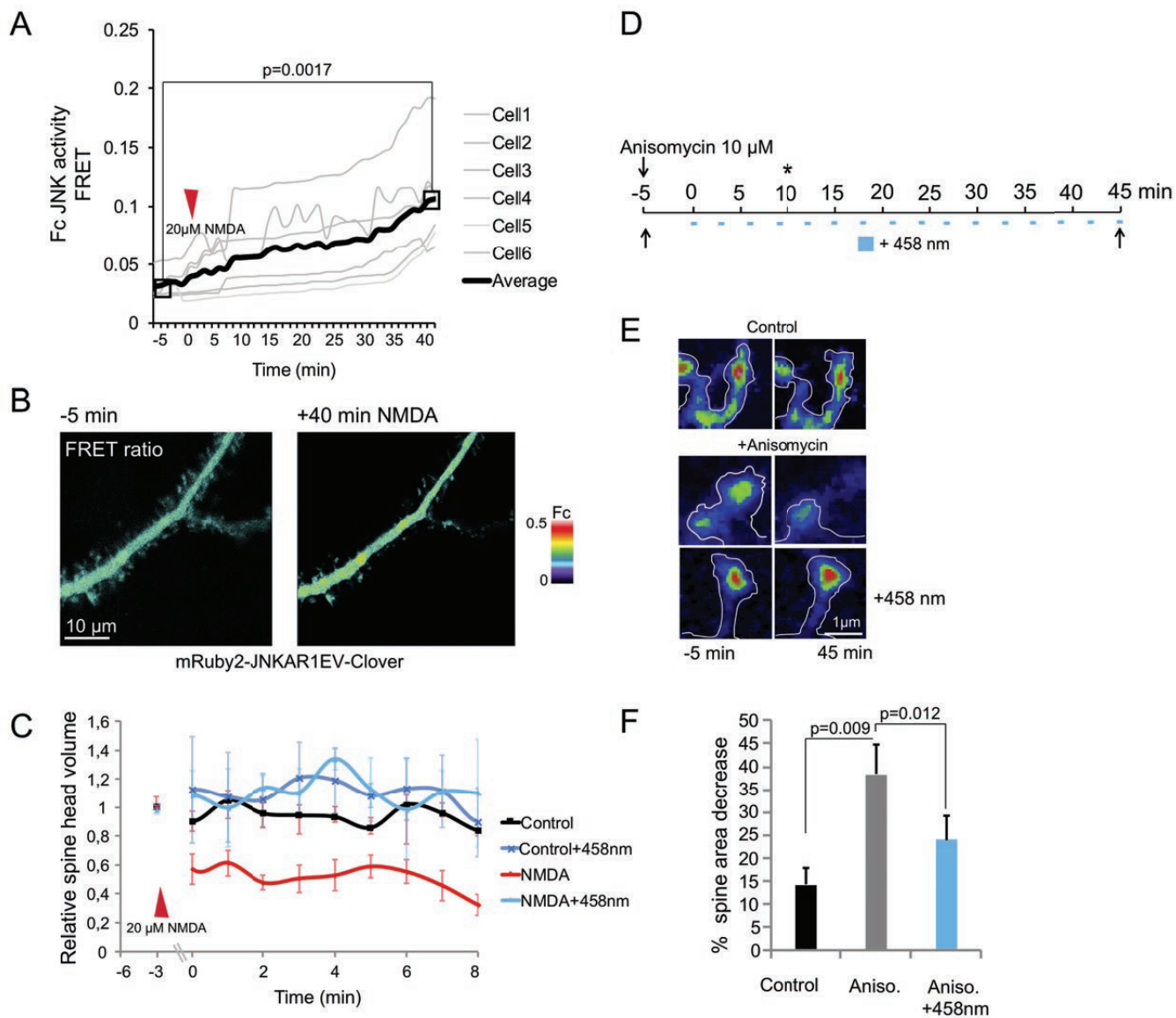


Figure 5

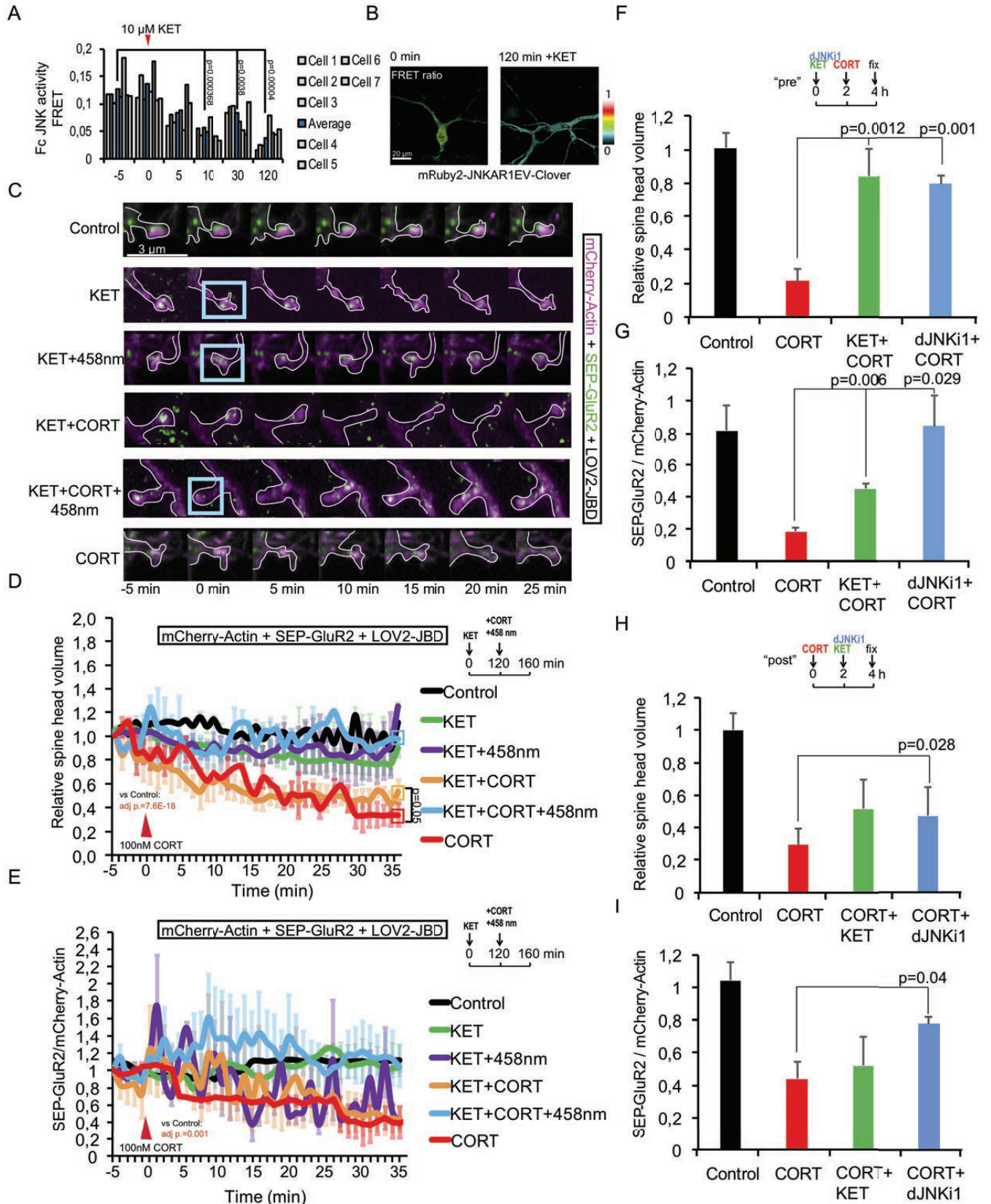


Figure 6